

## 4. Anatomy of a Fossil Subduction Channel – a quantitative view on changing structures along the plate interface

### Abstract

Modern concepts on processes of seismically active parts of converging plate interfaces are derived from lab experiments, theoretical inference, and geophysical observations, which have either poor resolution, or are strongly dependent on insufficiently constrained assumptions. We present observations from a continuous exposure of an ancient subduction channel in the depth range of its former seismogenic zone in the Central Alps of Europe related to Late Cretaceous - Early Tertiary subduction and accretion of the South Penninic lower plate underneath the Adriatic upper plate. The exposed plate interface has experienced flow and fracturing over an extended period of time reflecting a multistage evolution. Long-term mass transfer at the base of the Adriatic upper plate is controlled by tectonic erosion and accretion. We identify an unstable slip domain from pseudotachylytes in the temperature range between 200-300°C. This zone coincides with a domain of intense formation of mineralized veins in the subduction mélange. Mineralized veins as well as brittle fractures continue into the conditionally stable region below. The conditionally stable zone above the unstable slip area is devoid of mineralized veins, but displays ample evidence of fluid-assisted processes like the deeper zone: solution-precipitation creep and dehydration reactions in the mélange matrix, hydration and sealing of the base of the upper plate. Seismic rupture is possibly expressed by ubiquitous localized deformation zones. We hypothesize that sealing of parts of the seismogenic portion of the plate interface towards higher parts as well as reaction-enhanced destruction of upper plate permeability (e.g. growth of sheet silicates) is an important component localizing the unstable slip zone.

### 4.1. Introduction

To date, the plate interface of convergent plate boundaries cannot be directly accessed, but has been intensely studied, e.g. in Chile, with geophysical methods (e.g. Oncken et al., 2003; Krawczyk and the SPOC Team, 2003; Haberland et al., 2006), numerical modeling (e.g. Gerya et al., 2002; Gerya and Stöckhert, 2002) and sandbox simulations (e.g. Lohrmann et al., 2006). These, however, either have only poor resolution, or are strongly dependent on a number of poorly constrained assumptions. Hence, direct investigations of exhumed ancient convergent plate boundaries are requested to achieve insights into deformation processes

occurring along the plate interface despite multiple overprinting during exhumation. No continuous exposure exhibiting the complete seismogenic part of a subduction channel has been analyzed as yet. The here presented study contributes to the understanding of convergent plate boundaries in the depth range of their former seismogenic zone aiming at testing inferences and hypotheses of the various kinematic and mechanical concepts presented for the seismogenic zone. We use the complete exposure of this part of a former plate interface in the European Alps (Fig. 4.1), one of the best-studied mountain belts that has resulted from successive subduction, accretion and collision (Froitzheim et al., 1994; Handy, 1996; Schmid et al., 1996; Pfiffner et al., 2000).

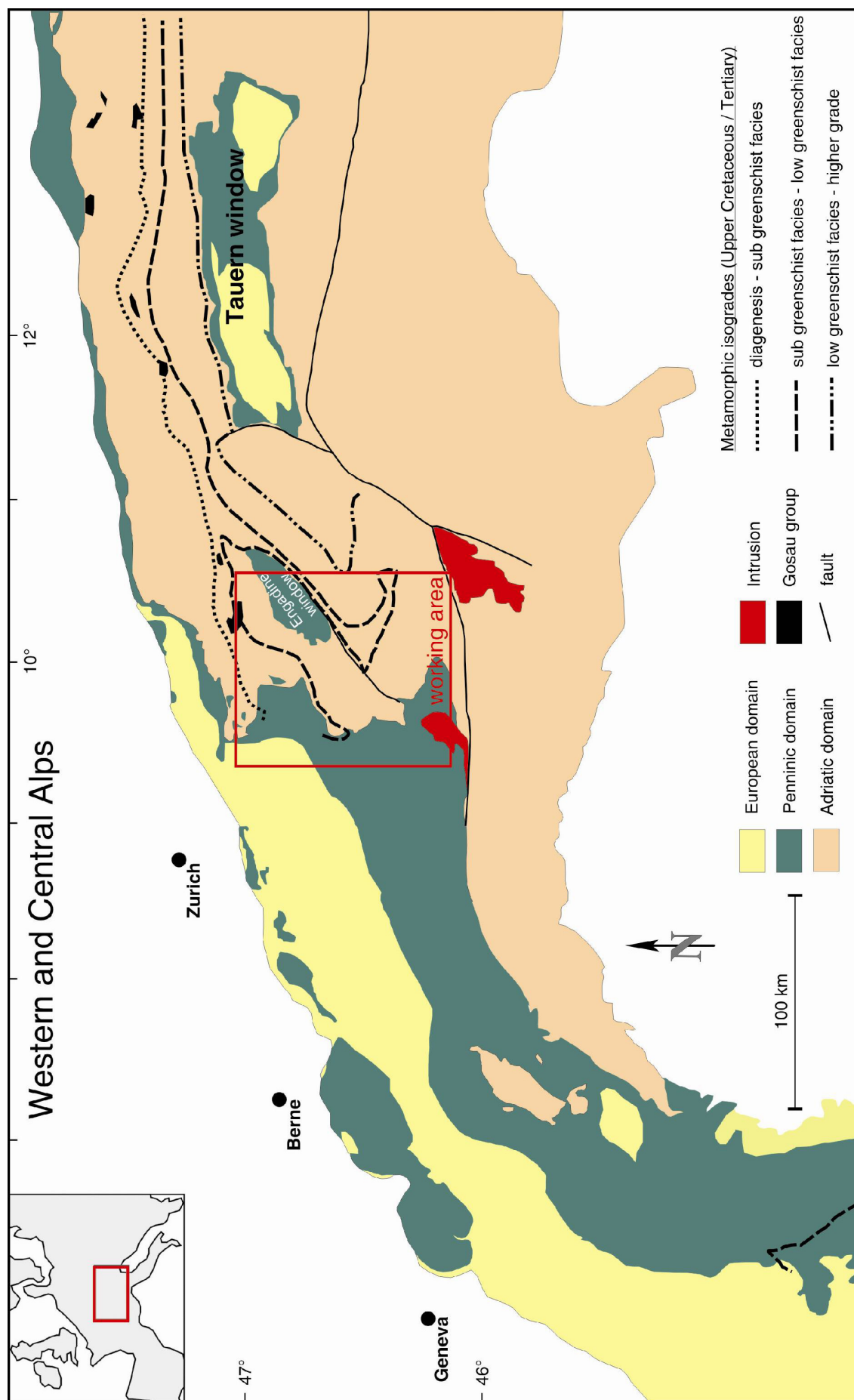


Figure 4.1: Simplified geological map of the European Alps, modified after Frey et al. (1974) and Stampfli et al. (2002). Metamorphic isogrades redrawn after Frey et al. (1999). Rectangle delineates the working area located along the transition of the Western to the Eastern Alps.



We analyzed a *mélange* zone (Fig. 4.1), which traces the plate interface zone of the fossil convergent plate margin.

This zone resulted from subduction of the Penninic ocean beneath the continental realm of the Adriatic plate (Austroalpine nappes) prior to the onset of collision with the European margin (Late Cretaceous - Early Tertiary, e.g. Froitzheim et al., 1996). Large-scale tilting during exhumation of the fossil plate interface provides access to various paleodepths and metamorphic conditions (Figs. 4.1, 4.2). The analysis of 8 transects crossing the former plate interface (Fig. 4.2) aims to identify the downdip variation of features along the former plate interface in terms of composition, deformation, and metamorphism. The exposed ancient plate interface has experienced flow and fracturing over an extended period of time, including minor overprint during collision and exhumation. Although this bears resemblance to active convergent plate margins that have been active over 10s of Myrs, our results invariably contain the effects of a multistage evolution.

## 4.2. Concepts of plate interface processes

### 4.2.1. *The subduction channel*

Cloos and Shreve (1988 a, b) have introduced the subduction channel concept denoting a zone between the upper and the lower plate of convergent plate margins. This zone may typically be up to a few kilometers wide, its material exhibiting a

velocity gradient towards both plates, and probably extending to a depth of more than 100 km (Gerya and Stöckhert, 2002). Material from both the oceanic and continental plate is transported downwards within the subduction channel, probably reaching mantle depths. Otherwise, material is partly off scraped and may either be accreted to the front of the accretionary wedge (frontal accretion), or to the base of the hanging wall (basal accretion) leading to duplex formation and antiformal stacking (e.g. von Huene and Scholl, 1991). Material may also be removed from the tip (frontal tectonic erosion) or the base (basal tectonic erosion) of the upper plate by tectonic erosion (e.g. Clift and Vannucchi, 2004). Subduction channels developing at erosive margins should be composed of deformed slope sediments, continental basement and cover-rocks in addition to the pelagic and hemipelagic sediments of accretive subduction channels. Strain localization in subduction channels may allow preserving original sedimentary and magmatic textures in blocks of all sizes. These units are bounded by a network of active shear zones or sheared matrix (Ábalos et al., 2003) that promote the downward transport of incoming material. Hence, the active subduction megathrust is not a stationary feature, but composed of transiently active interfaces within and at the boundaries of the subduction channel. While this concept provides a kinematic framework to assess the rock record exposed in an ancient subduction channel that has formed over geological time scales, it requires additional components to account for seismic cycle processes.

At shorter time scales unstable slip in the upper part of subduction channels occurs within a limited depth range along the plate interface, typically between 5 km and 45 km depth (Fig. 4.3, so-called seismogenic coupling zone, e.g. Ruff and Kanamori, 1983; Tichelaar and Ruff, 1993), causing major interplate

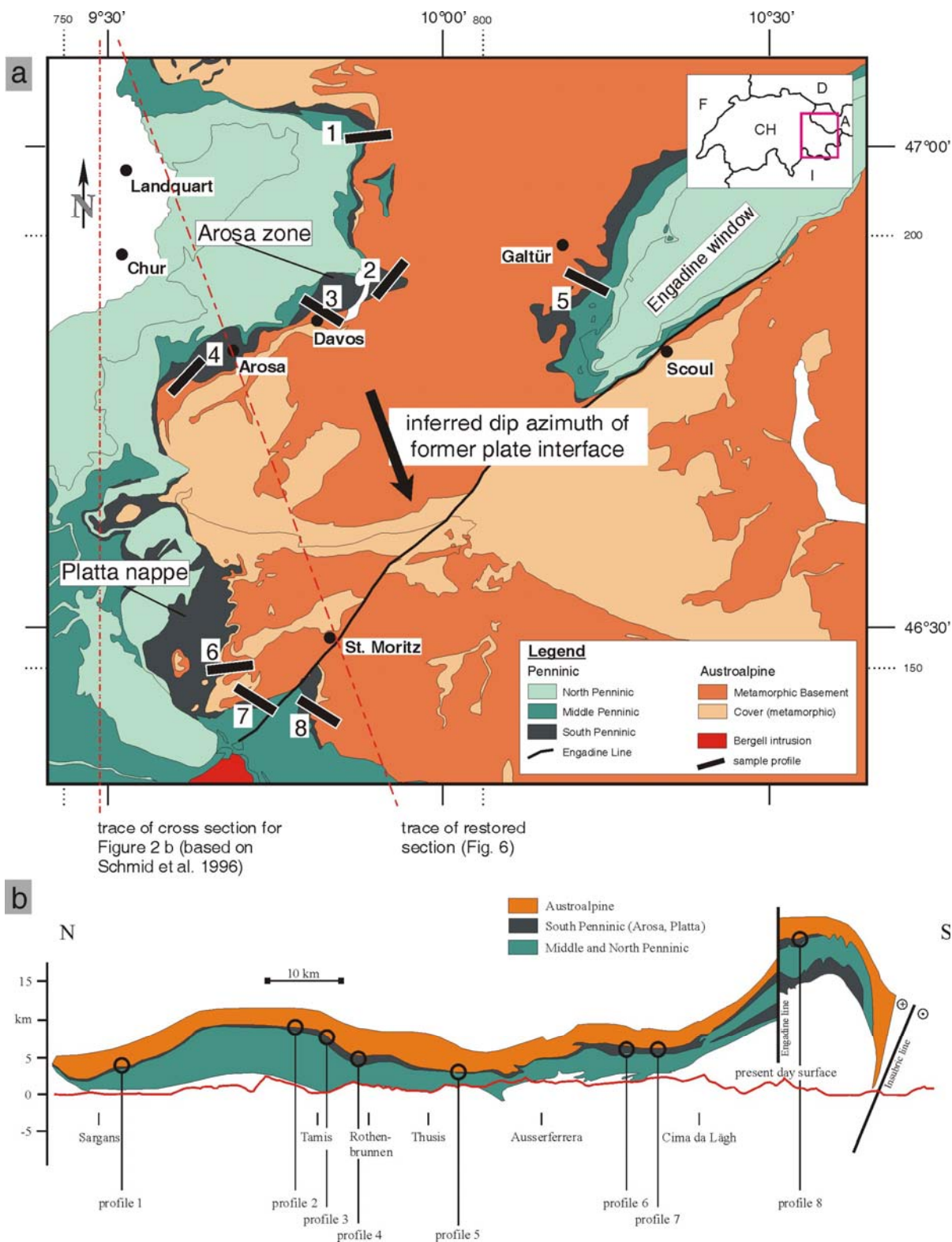


Figure 4.2: a) Tectonic map of the study area emphasizing the boundary zone between the South Penninic (dark green) and the Austroalpine (orange, part of the African plate). Numbers 1 to 8 refer to different profiles extending from domains of South Penninic origin into Austroalpine rocks. Arrow points to the former dip azimuth of the plate interface. Arosa zone and Platta nappe are local names for rocks of South Penninic affinity. Based on the Tectonic map of Switzerland 1:500.000, 2<sup>nd</sup> edition (1980).

b) Schematic profile of the Central Alps based on Schmid et al. (1996). Note the subdivision of the Penninic domain into a North Penninic ocean, Middle Penninic crystalline swell, and a South Penninic ocean.

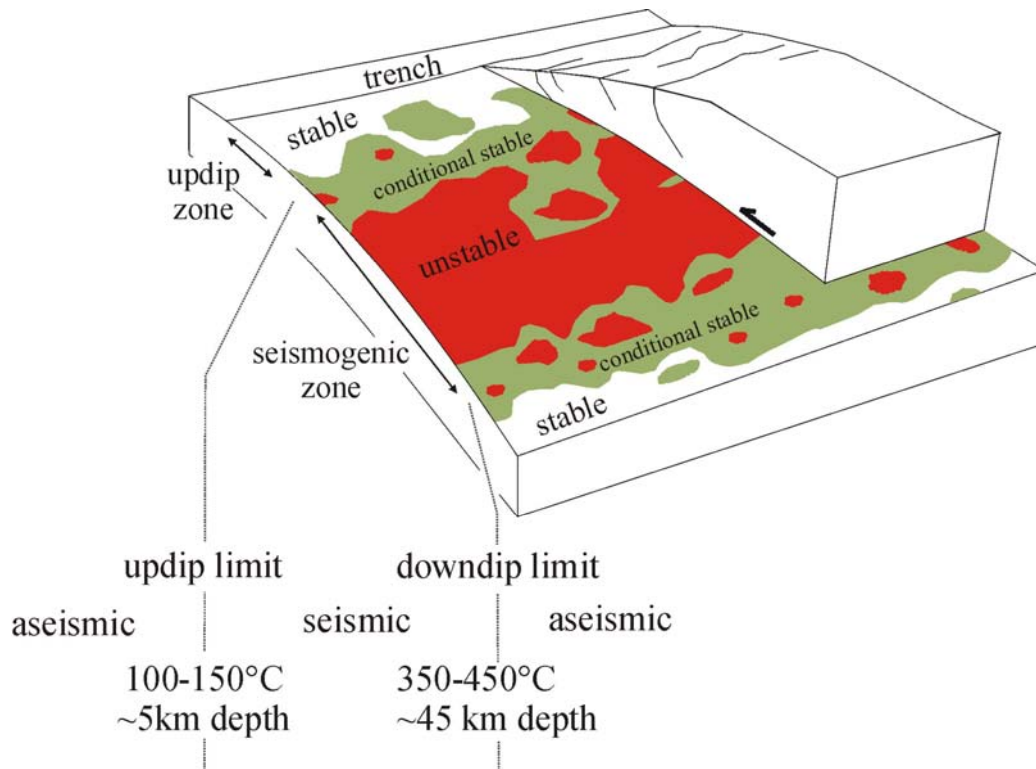


Figure 4.3: Schematic profile of the seismogenic zone of a convergent plate margin. The updip limit of seismogenic coupling (~5 km) is probably caused by consolidation, pressure solution or cementation changing the frictional behavior of the subducted material (Saffer and Marone, 2003). The downdip limit is located at about 45 km, and may be caused by the increasing dominance of ductile behavior (Nedimovic et al., 2003; Oleskevich et al., 1999) or the serpentinization of the forearc mantle (Hyndman et al., 1997; Peacock & Hyndman, 1999). Model of frictional conditions modified and extended downdip following Bilek and Lay (2002) delineating stable areas, conditionally stable and unstable regions. Note, these regions are variable in space and time due to their spatiotemporal-dependent causes (e.g. dehydration reactions). Therefore, no steady state conditions will be achieved along the plate interface zone.

earthquakes. The updip limit of the seismogenic coupling zone may be controlled by one or more of the following factors: dehydration of clay minerals, consolidation, pressure solution, cementation, alignment of sheet silicates, or upper plate geometry (e.g. Saffer and Marone, 2003). The proposed processes take place over a broad range of pressure and temperature conditions. Wang and Hu (2006) therefore state that the updip limit of seismogenic behavior must be a transitional feature. The downdip limit of the seismogenic zone is suggested to be controlled by changes in the geometrical setting of the subduction zone, the onset of viscous behavior of the deforming material (Oleskevich et al., 1999), or stable shearing

of serpentinized forearc mantle (Peacock and Hyndman, 1999).

#### 4.2.2. Mechanical concepts for coseismic and interseismic deformation

Scholz (1998) described different stability regimes along the plate interface (Fig. 4.3): a stable, an unstable, and a conditional stable regime. The stable regime exhibits velocity strengthening behavior, the unstable regime velocity weakening. Conditional stability defines a region, which exhibits a stable regime under quasistatic conditions. These patches are thought to be variable in space and time (Schwartz and Rokosky, 2007, and

references therein). According to Bilek and Lay (1998, 1999) seismic slip cannot be supported in the stable zone. There, elastic strain is relaxed by aseismic creep (Fig. 4.3). Earthquakes are only able to nucleate within unstable regions, but they can propagate into conditionally stable areas (Scholz, 1998; Moore and Saffer, 2001). The distribution of stable, unstable and conditional stable regions may be heterogeneous both downdip and along strike the plate interface producing islands of locked asperities embedded in weaker sedimentary material (Fig. 4.3) due to the heterogeneous character of subducted material, and the continuously occurring processes along the plate interface (e.g. cementation, dehydration).

Repeated thrust earthquakes as a result of a stick-slip frictional instability (Scholz, 1998; Moore and Saffer, 2001) require recovering after any slip event to compensate the coseismic strength drop and allow renewed accumulation of elastic strain. Fault healing by mineral precipitation, compaction, and fluid expulsion is usually invoked as the key process (e.g. Moore and Saffer, 2001).

Downward transported sediments strongly influence the physical properties of the plate interface, because they are less rigid than the rest of the subducting plate. Diverse sediment input in space and over geological times will lead to spatiotemporal modifications of the physical properties along the plate interface (i.e. frictional regimes). Bilek and Lay (1998, 1999) assumed that subducted sediments increase in rigidity and frictional resistance due to compaction, and are therefore responsible for unstable slip, and for the decrease of source durations in earthquake rupturing. Scholz (1998) reported a velocity strengthening behavior for less consolidated sediments, possibly promoting areas of stable sliding (Fig. 4.3). Compaction and phase transitions within both sediments and the subducting slab

lead to dewatering and dehydration, providing fluids to the plate interface system. This water release increases the pore pressure, and therefore reduces normal stress and effective friction increasing the probability of fracture formation. Further down the plate interface loss of fluids increases the strength of the sediments. The replacement of clay minerals by zeolite or quartz enforces velocity weakening due to the velocity weakening behavior of low-porosity rocks and framework silicates (Moore and Saffer, 2001), thus increasing the probability of earthquakes. Whether this change is abrupt or gradual is mostly defined by the general permeability along the plate interface.

### 4.3. Geological setting

#### 4.3.1. *Alpine Evolution*

The European Alps resulted from the collision of the European and the Adriatic continental plates and southeastward to southward subduction and accretion of the intervening Penninic oceanic domain. The oceanic units sandwiched between both continental plates were partly accreted to the base of the overriding continental Adriatic margin (Figs. 4.1, 4.2) (Bousquet et al., 1998). The Penninic domain consists of two oceanic basins related to the Alpine Tethys (North Penninic Valais basin and South Penninic ocean), divided by the so-called Briançonnais continental swell (Middle Penninic) (Fig. 4.2) (e.g. Florineth and Froitheim, 1994, and references therein). These units were successively subducted and accreted to the Austroalpine domain (Adriatic plate) since the Late Cretaceous until the final collision of the Adriatic plate with the European plate during the Middle Tertiary.

Most models differentiate two phases of subduction during Alpine orogeny:

Cretaceous subduction is defined by an east to southeast dipping subduction zone (e.g. Bousquet et al., 1998; Pfiffner et al., 2000), and associated top-W, locally top-SW and top-NW thrusting (Froitzheim et al., 1994; Handy, 1996). The direction of convergence changed to north – south during the Tertiary with top-N thrusting (Froitzheim et al., 1994; Handy, 1996). According to Ring (1989) structures of top-N thrusting should be more pronounced towards structurally deeper levels of the Penninic domain. The shift between E/SE- to S-directed subduction is associated with NW-SE directed extension, top-SE shearing and normal faulting during the Late Cretaceous affecting the upper plate and partly the structural higher levels of the Penninic domain. This may locally overprint older structures (folds and faults), and reactivate preexisting fault planes (Silvretta basal thrust) of the preceding top-W directed stage of thrusting (Froitzheim et al., 1994). Comparing with recently active convergent plate margins, both orogenic stages can be seen to be the consequence of continuous oblique subduction and accretion of the Penninic domain underneath the Adriatic plate with migration of deformation towards the foreland, which culminated in the collision with the European margin.

#### 4.3.2. *Geology of the working area*

The working area is located along the transition from the Western to the Eastern Alps (Figs. 4.1, 4.2). The main geological units are represented by the Penninic and Austroalpine domain. In the working area remnants of the South Penninic ocean are represented by the Arosa zone (northern area, Fig. 4.2) and Platta nappe (southern area, Fig. 4.2). The upper plate (Adriatic plate) consists of the Austroalpine nappe stack including the Silvretta, Ötztal, Julier and Err-Bernina nappes, all of them built from continental basement covered by Permo-Mesozoic sediments. The boundary

between the South Penninic domain and the Austroalpine is commonly interpreted as a Late Cretaceous suture (e.g. Handy, 1996).

The Arosa and Platta nappes form a *mélange* zone of intensely deformed oceanic and continental material (Deutsch, 1983; Ring et al., 1988; and references therein; we treat “*mélange*” as a scale- and origin-independent descriptive term for an internally fragmented complex that contains blocks of various origin in a sheared matrix; see Ring et al. (1990) and Cowan (1985)), suggesting that the plate interface is a broad deformation zone rather than a discrete suture. The *mélange* is mainly composed of Jurassic ophiolites, radiolarian chert, pelagic limestone, shale and sandstone (Ring et al., 1988). Competent blocks of Austroalpine and Penninic affinity are embedded in the incompetent shaly or serpentized matrix (Ring et al., 1990). The large-scale structures of the Arosa zone are construed by e.g. Ring et al. (1988, 1989, 1990) as the deep parts of an accretionary wedge formed at the tip of and below a thrust belt migrating towards the west.

#### 4.3.3. *Age constraints and metamorphism*

Subduction of the ophiolites from the South Penninic ocean, originally formed during the Jurassic (200 Ma to 180 Ma, Ring, 1989;  $163.5 \pm 1.8$  Ma and  $164.0 \pm 2.7$  Ma, Gebauer, 1999), initiated at around 120 Ma to 100 Ma (Fig. 4.4, Handy and Oberhänsli, 2004, and references therein). Flysch deposits found in the Arosa and Platta nappes show ages ranging from Aptian to Cenomanian (late Early Cretaceous to early Late Cretaceous; Ring, 1989, and references therein). No younger sediments are recorded within the South Penninic domain. The rocks composing the footwall of the South Penninic domain are formed by flysch deposits derived from

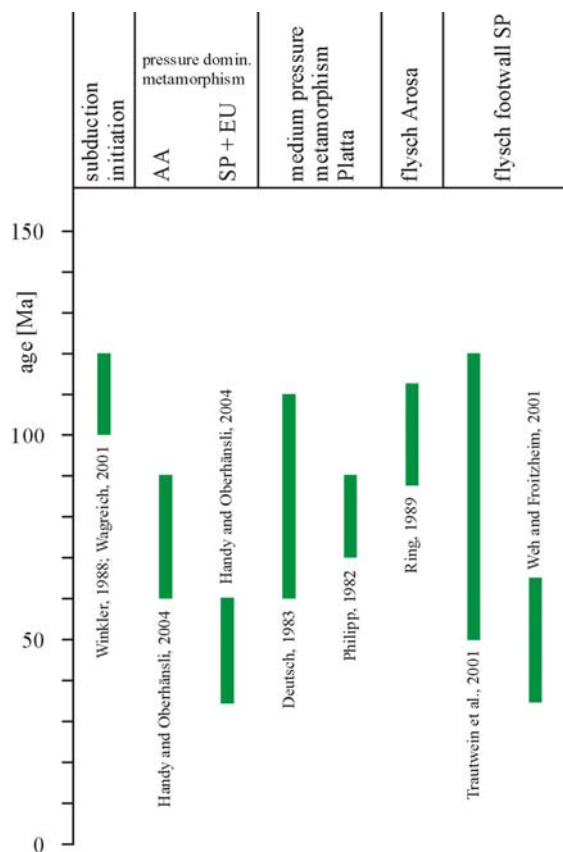


Figure 4.4: Compilation of geochronological data available for the study area concerning the subduction and accretion of the South Penninic domain (SP), deformation within the Austroalpine nappe stack (AA), and flysch deposition within the South Penninic domain and its footwall. EU = European plate.

Middle and North Penninic units, and from the distal European margin (e.g. Rhenodanubian flysch). Biostratigraphic evidence from these flysch deposits yields an Early Cretaceous to early/ middle Eocene age (Trautwein et al., 2001) (Fig. 4.4). In addition, Weh and Froitheim (2001) reported that the youngest sediments in the footwall of the Arosa zone are Paleocene to possible Eocene in the Middle Penninic Falknis nappe. Hence, subduction-related deformation along the boundary zone between the South Penninic and Austroalpine nappes lasted at least until the Late Cretaceous (end of sedimentation signaling passage through the trench area) to the early/ middle Eocene (where latest sedimentation occurred within the flysch accreted at the

base of the South Penninic units), roughly between 89 Ma to 50 Ma. The northwestward younging of flysch deposition is consistent with a migration of subduction-related accretion towards the northwest (e.g. Handy and Oberhänsli, 2004; and references therein). The general time scheme is also supported by isotopic ages showing 90 Ma to 60 Ma for pressure-dominated metamorphism of the Lower Austroalpine units, and 60 Ma to 35 Ma for the South Penninic and European units, respectively (Handy and Oberhänsli, 2004; and references therein) (Fig. 4.4). Constraints for the timing of pseudotachylyte formation along the fossil plate interface immediately above the base of the Austroalpine nappe stack are given by Thöni (1988). He presented Rb/Sr data from pseudotachylytes collected along the northwestern part of the Engadine window (close to profile 5, Fig. 4.2), which resulted in ages of approximately 75 Ma.

Metamorphic conditions of South Penninic rocks range from upper diagenetic or lowermost greenschist facies in the north of the working area, to middle to upper greenschist facies in the southern parts (Fig. 4.1). A compilation of published geothermobarometric data is given in Table 1. Metamorphic isogrades for the above time span generally trend WSW-ENE in the Central Alps (Frey and Ferreiro Mählmann, 1999; Handy and Oberhänsli, 2004) (Fig. 4.1) providing a crude indication for the trend of the former Adriatic plate margin.

#### 4.4. Methods

We measured foliation, lineation, shear bands, tension gashes, folds, faults, their density, geometric proportions, and their relative age relationships at a series of 8 selected profiles from north to south (Figs. 4.2, 4.5). We additionally used structural data published by numerous authors (e.g. Froitheim et al., 1994; Ring, 1989). We

Table 1. Compilation of database for section restoration.

distance from corrected trench tip [km]	location	method	comments	R <sub>max</sub> [%]	Si p.f.u.	T [°C]	P [kbar]	P <sub>cor.</sub> [kbar]	converted depth [km]	references
56.8	southern termination of Wägitaler flysch	vitrinite reflectance (effective maturation time 20 Ma)	data converted to depth using different geothermal gradients	1.8		180			7.2 - 12.0	Ferreiro Mähimann 1994
58	south of Bargella	vitrinite reflectance (effective maturation time 20 Ma)	data converted to depth using different geothermal gradients	2.1		190			7.6 - 12.7	Ferreiro Mähimann 1994
60.9	close to Steg	vitrinite reflectance (effective maturation time 20 Ma)	data converted to depth using different geothermal gradients	2.7		225			9.0 - 15.0	Ferreiro Mähimann 1994
65.2	Profile 1	vitrinite reflectance (effective maturation time 20 Ma)	data converted to depth using different geothermal gradients	2.9		230			9.2 - 15.3	Ferreiro Mähimann 1994
65.2	Profile 1	temperature dependent deformation observed at different minerals	pressure solution in carbonates, brittle deformed			150			6.0 - 10.0	
80.5	between profiles 1 and 2	fluid inclusion data					2.3 - 4.2		8.7 - 15.9	Ring et al. 1989
93.3	Profile 3	vitrinite reflectance (effective maturation time 20 Ma)	data converted to depth using different geothermal gradients	3.2		236			9.4 - 15.4	Ferreiro Mähimann 1994
97	between profiles 3 and 4	illite crystallinity				300 - 350			12.0 - 23.3	Ring 1989
97	between profiles 3 and 4	fluid inclusion data					2.5 - 5.2		9.5 - 19.7	Ring et al. 1989
98.2	Profile 4	vitrinite reflectance (effective maturation time 20 Ma)	data converted to depth using different geothermal gradients	3.9		240			9.6 - 16.0	Ferreiro Mähimann 1994
113.6	close to Tiefencastel	vitrinite reflectance (effective maturation time 20 Ma)	data converted to depth using different geothermal gradients	4.3		245			9.8 - 16.3	Ferreiro Mähimann 1994
114	south of profile 4	illite crystallinity, vitrinite reflectance					2.0 - 4.0		7.6 - 15.1	Frey and Ferreiro Mähimann 1999
125.2	Profile 5	vitrinite reflectance (effective maturation time 20 Ma)	data converted to depth using different geothermal gradients	4.5 - 5.0		247 - 249			9.9 - 16.6	Ferreiro Mähimann 1994
137.8	Profile 6	vitrinite reflectance (effective maturation time 20 Ma)	data converted to depth using different geothermal gradients	5.0 - 5.5		249 - 255			10.0 - 17.0	Ferreiro Mähimann 1994
137.8	Profile 6	chlorite thermometry				308 - 325			12.3 - 21.7	Ferreiro Mähimann 2001
137.8	Profile 6	Si content in phengite	minimum pressure	3.32			3.5 - 6.0		13.2 - 22.7	Ferreiro Mähimann 2001
163.8	Profile 8	temperature dependent deformation observed at different minerals	calcmylonites, intracrystalline deformation of quartz, brittle deformed feldspar			350 - 450			14.0 - 30.0	
163.8	Profile 8	greenschist facies assemblage				300 - 350			12.0 - 23.3	Handy et al. 1996
163.8	Profile 8	Si content in phengite	minimum pressure, recalibrated after Massonne and Szpurka 1997	3.41			8.0 - 9.0	5.0	18.9	Handy et al. 1996

estimated pressure conditions of samples from both the base of the Austroalpine nappe stack and the South Penninic domain in order to restore former plate geometry and the position of the individual profiles. Data for the Austroalpine basement rocks are only useful for our study, where the overprint of the pre-Alpine mineral assemblage is almost complete. This is the case for profiles 6, 7 and 8 (see Chapter 4.5.1.). We make use of the Si-content of phengite due to the Tschermak's substitution with the graphical solution provided by Massonne and Szpurka (1997).

Table 2. Microprobe analyses of phengite of different samples.

sample	B-4	C-15	C-12	B-8	B-13	B-32
Profile	6	7	7	8	8	8
analyses (n)	24	8	4	11	5	22
mineral	phg	phg	phg	phg	phg	phg
SiO <sub>2</sub>	50.12	49.24	51.20	51.26	50.17	47.70
TiO <sub>2</sub>	0.19	0.17	0.06	0.11	0.38	0.13
Al <sub>2</sub> O <sub>3</sub>	25.85	29.78	28.39	25.95	24.81	31.73
MgO	2.37	2.20	3.25	3.18	3.14	2.21
CaO	0.01	0.00	0.01	0.01	0.01	0.07
MnO	0.05	0.04	0.03	0.04	0.03	0.01
FeO	5.14	4.51	3.95	3.88	5.30	2.16
Na <sub>2</sub> O	0.08	0.34	0.15	0.00	0.05	0.29
K <sub>2</sub> O	10.97	9.80	10.77	10.23	10.91	9.51
Total	94.77	96.08	97.81	94.64	94.79	93.80
Formula proportions						
Si	3.421	3.282	3.355	3.457	3.430	3.215
Al <sup>IV</sup>	0.579	0.718	0.645	0.543	0.570	0.785
[Z]	4.000	4.000	4.000	4.000	4.000	4.000
Al <sup>VI</sup>	1.500	1.621	1.547	1.519	1.428	1.735
Ti	0.009	0.009	0.003	0.005	0.019	0.006
Fe <sup>2+</sup>	0.293	0.251	0.216	0.219	0.303	0.122
Mn	0.003	0.002	0.002	0.002	0.002	0.001
Mg	0.241	0.219	0.317	0.320	0.320	0.221
[Y]	2.046	2.102	2.086	2.066	2.072	2.086
Ca	0.001	0.000	0.001	0.000	0.000	0.005
Na	0.011	0.044	0.019	0.000	0.007	0.038
K	0.955	0.833	0.900	0.881	0.952	0.817
[X]	0.966	0.877	0.920	0.881	0.959	0.860
Cat. Charge	22.000	22.000	22.000	22.000	22.000	22.000
Mg#	0.451	0.47	0.59	0.595	0.514	0.647
X <sub>Fe</sub>	0.882	0.90	0.85	0.844	0.844	0.894
X <sub>Mg</sub>	0.118	0.10	0.15	0.155	0.154	0.106

Due to the absence of critical mineral assemblages for which this geobarometer was calibrated (K-feldspar + phlogopite + quartz, quartz + garnet + kyanite, talc + kyanite + quartz), this method only yields minimum pressure conditions. One sample from profile 6, two samples from profile 7,

and three samples from profile 8 were selected for electron microprobe analyses. Mineral analyses were performed using a CAMECA SX100 electron microprobe operating in the wavelength-dispersive mode. Major and minor elements were determined at 15 kV acceleration voltage and a beam current of 20 nA with counting times of 20 s for major elements, and 30 s for minor elements. The beam diameter used for the mineral analyses was 5 µm for all mineral except for plagioclase, where we used 10 µm in order to suppress sodium diffusion. The standard sets of the Smithsonian Institute (cf. Jarosewich et al., 1980) and of MAC<sup>TM</sup> were used for reference. Table 2 lists samples, and the results of analyses. Mineral abbreviation in the text and Tables follow Kretz (1983). Field images were processed with the image-processing software Scion Image for fabric quantification. Afterwards, the software automatically outlined, counted and measured the individual clasts yielding their major and minor axes, and the clast size.

## 4.5. Observations and results

### 4.5.1. Structural data

Rocks of the Arosa zone and Platta nappe close to the contact to the hanging wall Austroalpine nappes (at least in the first few hundred meters) suffered a penetrative deformation with an inferred direction of tectonic transport changing gradually from top-NW in the north of the working area to top-SW in the southernmost parts (Fig. 4.5). Foliation planes dip moderately toward SE to NE and associated stretching lineations plunge smoothly toward SE and ENE, respectively. These structures are best developed in the south of the working area. Embedded clasts within the metasedimentary matrix of the South Penninic domain are partly bounded by

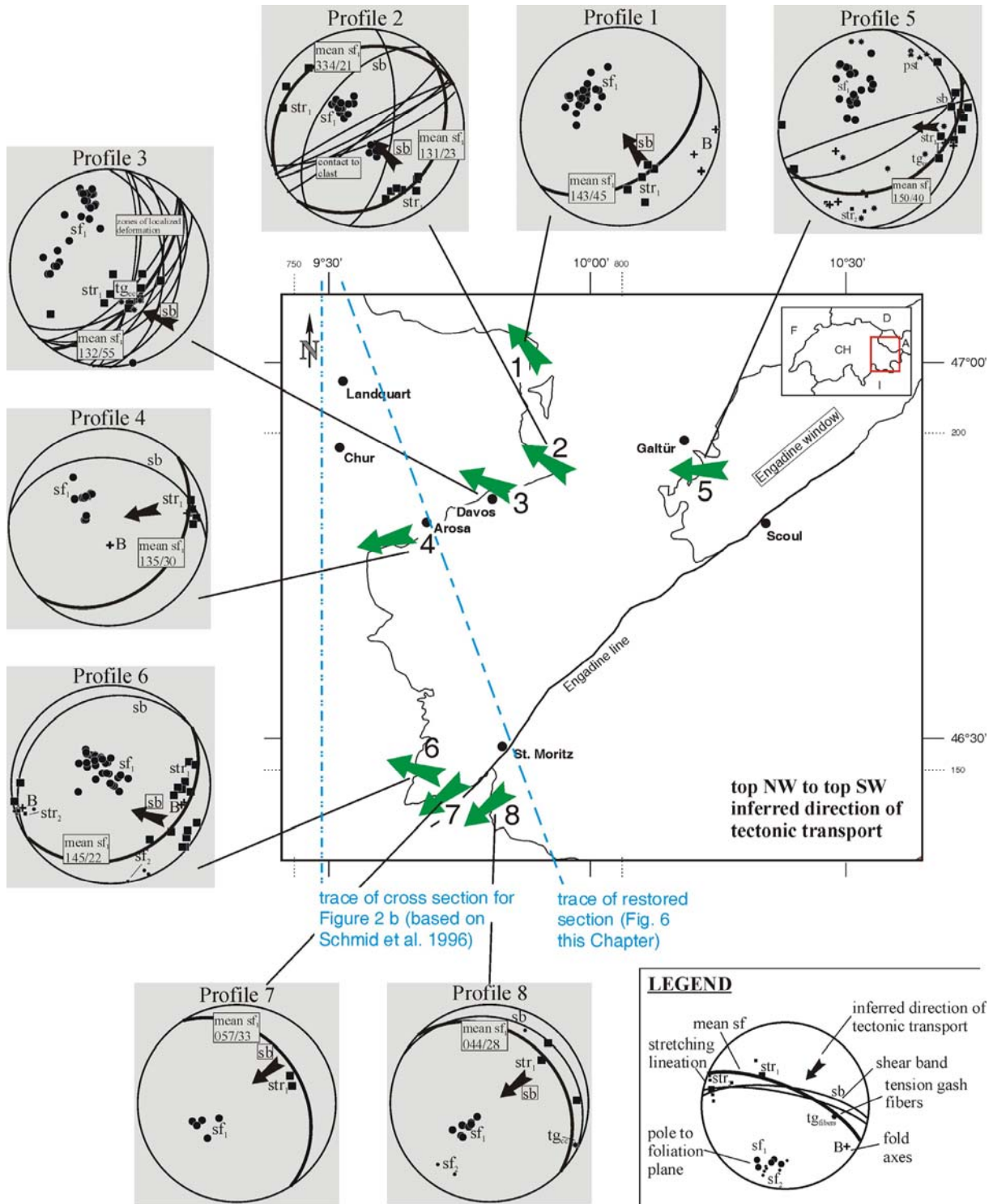


Figure 4.5: Structural data of brittle-ductile to ductile deformation associated with pervasive fabric showing top-NW to top-SW direction of tectonic transport (generally top-W). All plots are Schmidt net lower hemisphere, equal-area diagrams. Due to similarity of structural data along each profile, diagrams are a combination of several outcrops at every profile.

shear zones, which consistently show a general top-W directed tectonic transport.

Deformation with general top-W directed tectonic transport of the Austroalpine basement (upper plate) in the northern part of the study area is expressed by microscale fracture zones reactivating the preexisting foliation of probably Variscan age. This Alpine overprint increases towards the south. At profiles 6, 7 and 8 Alpine deformation pervasively overprints the preexisting foliation within the upper plate basement close to the boundary zone to the South Penninic domain. There, growth and recrystallization of sheet silicates (mainly white mica) occurred parallel to the preexisting foliation. Orientation of foliation in the Austroalpine rocks parallels its corresponding foliation within the South Penninic domain, at least in the first few hundred meters above the base of the hanging wall, and both consistently parallel the base of the Austroalpine nappe stack. Deformation of the South Penninic domain increases towards the south of the working area as expressed by a more distinct foliation with a narrower spacing, and the progressive obliteration of sedimentary structures.

Structures indicating the general top-W tectonic transport are overprinted by subsequent deformation with significantly lower intensity. It is localized in distinct bands or sometimes present as a spaced cleavage (see also Ring, 1989; Dürr, 1992). We also observed brittle-ductile shear bands with top-E to top-SE directed tectonic transport, which are more pronounced towards the south, and seem to reactivate the preexisting top-W structures. These structures are again overprinted by top-N thrusting, which can be inferred from roughly E-W orientated fold axes of open folds at various scales, folding the above older structures. Steeply dipping strike-slip faults (dextral E-W trending faults with offsets of up to 500m, sinistral N-S trending faults with offsets less than

100m) represent the late stage of brittle deformation affecting the whole working area (Ring, 1989).

#### 4.5.2 Geobarometry and temperature estimates

Analyses of white mica (phengite) resulted in a Si-content ranging from 3.215 p.f.u. to 3.457 p.f.u. (Table 2) corresponding to minimum pressures around 3 - 4 kbar at profile 6 and profile 7, and 3 - 6 kbar at profile 8, assuming a temperature of 300°C to 350°C (supported by subgrain rotation recrystallization of quartz). Recalibration of the data provided by Handy et al. (1996) using the graphical solution of Massonne and Szpurka (1997) resulted in about 5 kbar minimum pressure for the base of the upper plate at profile 8, which is substantially lower than the minimum pressures of 8 - 9 kbar suggested by Handy et al. (1996). Deformation temperatures are inferred from macroscopic and microscopic observations concerning the deformational behavior of carbonate minerals, quartz and feldspar. They point to a temperature of about 150°C in the north (pressure solution of carbonates, fractured quartz) and 350°C to 400°C in the south of the working area (calcmylonites, subgrain rotation recrystallization in quartz, brittle deformation of feldspar). These results corroborate published data (Ferreiro Mählmann, 2001; Frey and Ferreiro Mählmann, 1999; Handy et al., 1996; Handy and Oberhänsli, 2004; Ring, 1989; Ring et al., 1989) (Table 1).

#### 4.6. Restoration of the fossil plate interface

In order to relocate plate interface features to their former position along the plate interface we projected the investigated profiles into a composite synthetic section perpendicular to the strike of the former

subduction zone. This restoration is based on the N-S section provided by Schmid et al. (1996), redrawn after the NFP-20-East seismic traverse covering the main geological and tectonical units in the working area (Fig. 4.2b). We used the software 2DMove (Midland Valley) for restoration. The fossil strike of the subduction zone is roughly constrained by the above mentioned orientation of the metamorphic isogrades associated with Late Cretaceous to Early Tertiary subduction and accretion of the Penninic domain, which trends WSW-ENE (Fig. 4.1). In addition, the present day general trend of the external Gosau basins that represent Late Cretaceous forearc basins developed on the Northern Calcareous Alps, show the same trend (Fig. 4.1, Sanders and Höfling, 2000; Wagneich and Krenmayr, 2005). According to Wagneich (1995), Wagneich and Decker (2001) and Wagneich and Krenmayr (2005) the Gosau basins represent subsiding slope basins at the front of the upper plate controlled by oblique dextral convergence. In consequence, we assume the downdip azimuth of the former plate interface to be SSE requiring projection of the geological units and profile positions from the N-S section into a new section rotated by 20°. The first step in restoration was the removal of the vertical offset along the Engadine line (Figs. 4.2, 4.6a) using “fault parallel flow” as deformation algorithm. In a second step “line length unfolding” was applied to the folded South Penninic domain, which resulted in two flat lying horizons (Fig. 4.6a).

The minimum distance of the fossil trench north from profile 1 is given by the present day position of the Wägitaler flysch, which represents remnants of the Early Tertiary accretionary prism, accreted to the tip of the wedge and at the base of the South Penninic domain (Tectonic map of Switzerland 1:500.000, 2<sup>nd</sup> edition, 1980). We assume the exposed northern limit of the Wägitaler flysch as the minimum

position of the former trench because of possible erosion of its toe and of possible syncollisional shortening. We extended the restored section adding the distance between the northern end of the South Penninic domain in Fig. 4.2 and the northern limit of the Wägitaler flysch (Fig. 4.6a).

The dip of the ancient plate interface zone (i.e. the megathrust) is reconstructed from depth conversion of all geobarometric data using a mean density of 2.7 g/cm<sup>3</sup> (i.e. 1 kbar corresponding to 3.78 km below surface) and plotting them into the restored and rotated section assuming a mean topographic slope of 5° for the outer forearc wedge and 3° for the inner forearc wedge (Fig. 4.6b, Table 1) referring to Wang and Hu (2006). They reported a steeper slope for the outer wedge compared to the slope angle of the inner wedge, and the transition between outer and inner wedge is situated close to the updip limit of seismogenic coupling (approximately 30 – 40 km landward of the trench tip). The assumed slope angles are also comparable to values presented by Clift and Vannucchi (2004), which reported a mean forearc slope of 5° for erosive margins (cf. compilation of global forearc slopes by Moores and Twiss, 1995). Landward of the shelf edge (corresponding to about 200m water depth) we used a topographic slope of 0° in order to reach the shoreline close to the downdip limit of the seismogenic coupling zone (Hyndman et al., 1997). Additionally, depth conversion for all geothermometric data was performed assuming different geothermal gradients. For estimating the geothermal gradient we used heat flow data presented by Grevemeyer et al. (2005) with an average value of 30 mW m<sup>-2</sup> for a region landward of the trench, and a thermal conductivity for granites (1.5 to 2.5 W m<sup>-1</sup> K<sup>-1</sup>) and sediments (1.5 to 5 W m<sup>-1</sup> K<sup>-1</sup>) (Clauser and Huenges, 1995), most likely the components of the fossil convergent plate margin within the study

area. This resulted in an average geothermal gradient of 15 to 25 °C km<sup>-1</sup>.

For additional constraints in estimating the dip of the fossil plate interface we reevaluated vitrinite reflectance data provided by Ferreiro Mählmann (2001). We constructed a subsidence curve assuming approximately 10 km of burial for the mean of the used rock samples, and a time range between 90 Ma and 30 Ma for maturation of the organic material (see also Chapter 4.3.3). This resulted in about 20 Ma effective time of maturation assuming a polynomial interpolation of the used data points. Using this value and the diagram provided by Bostick et al. (1979) the vitrinite reflectance data can be transformed into temperature information, and thus, using again different geothermal gradients, into depth values. Vitrinite reflectance data north of profile 1 point to an Early Tertiary overburden of at least 7 km. Therefore, the previously assumed minimum extent of the accretionary prism using the tip of the Wägitaler flysch was underestimated. In consequence, we shifted the adjusted tip of the fossil accretionary prism further towards the north (Fig. 4.6b).

The former plate interface is constructed by pinning the plate interface at the tip of the former wedge, and extending the plate interface through the mean of the geothermobarometric data. Where geobarometry points to minimum pressure

conditions we plotted the interface below the deepest minimum pressure datapoint. This procedure resulted in a constant slab dip angle of approximately 8° (Fig. 4.6c). Global data for slab dips for the first 100 km from the trench are in a similar order of magnitude (Lallemand et al. 1994; Moores and Twiss, 1995; Clift and Vannucchi, 2004). The resultant distances for each profile relative to the trench are shown in Fig. 4.6c.

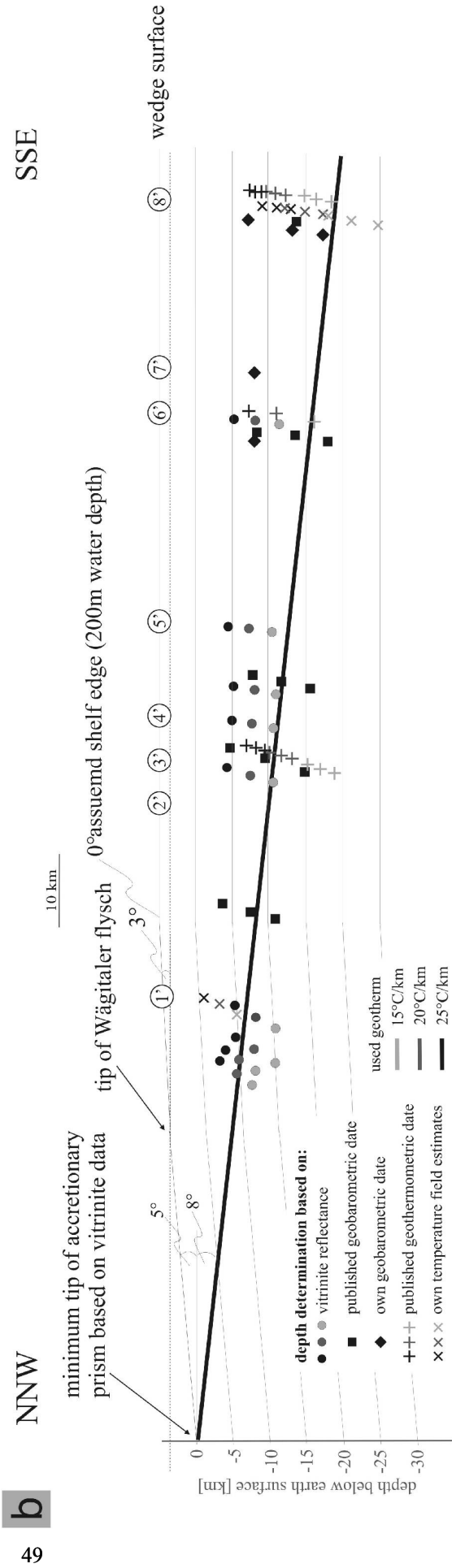
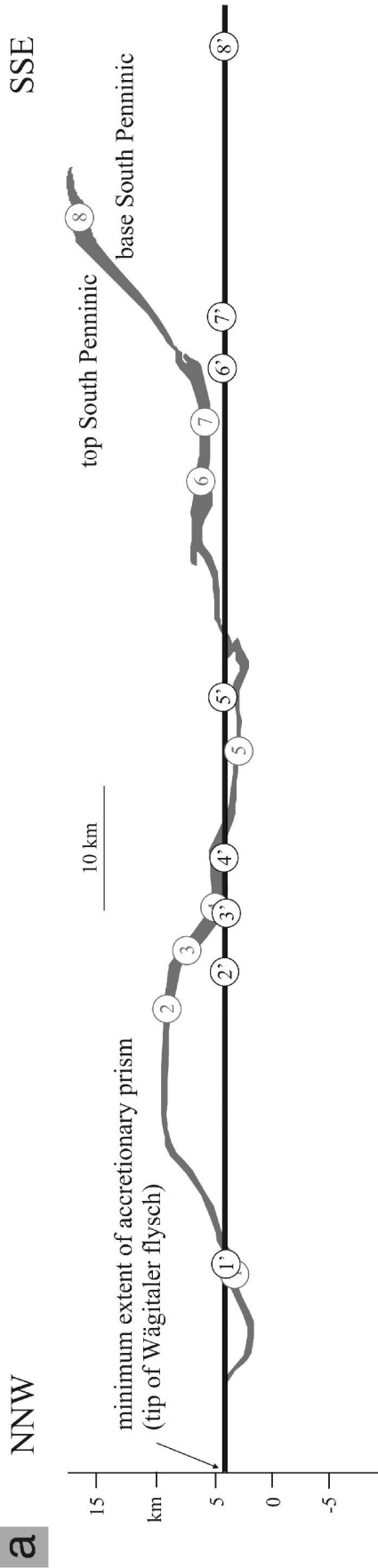
#### 4.7. Spatial variation of characteristics along the fossil plate interface

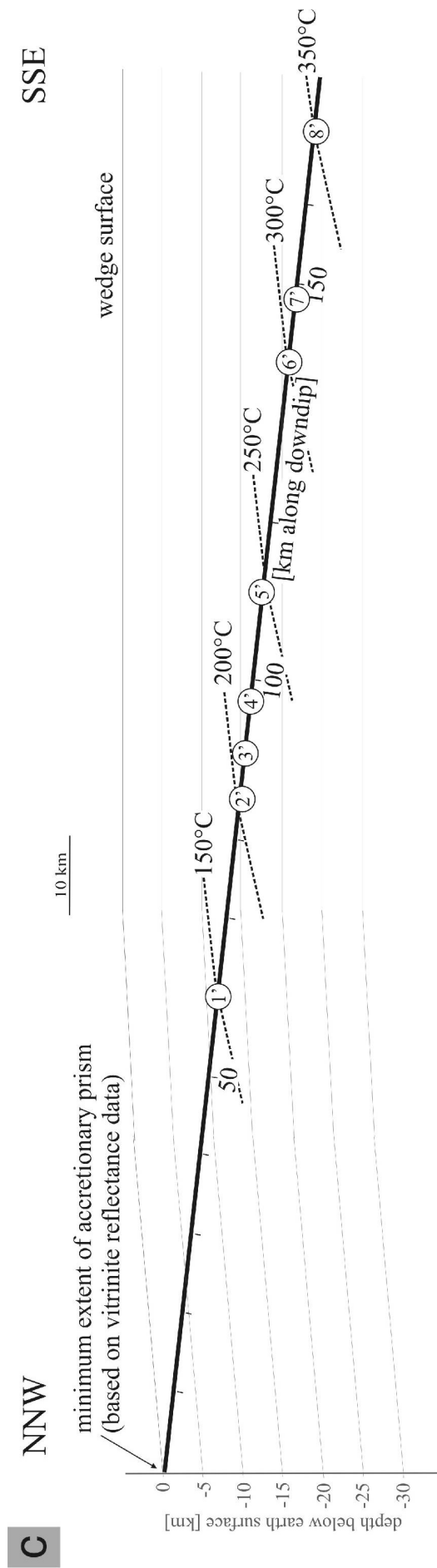
##### 4.7.1. General information

The apparent thickness of the South Penninic mélange varies from a few tens of meters up to more than 2500 m, either reflecting their original thickness after abandoning this shear zone following basal accretion of the mélange or a reduction from subsequent thinning. Within the matrix of shales and serpentinites clasts of more competent material are incorporated, originating either from the Austroalpine upper plate (crystalline basement, its sedimentary cover), or formed by slivers of the lower plate (metagabbros, metabasalts, the sedimentary deposits of the ocean floor, or the trench fill turbidites).

In contrast to the compositional homogeneity in all transects, other features

Figure 4.6: Section restoration using 2DMove (Midland Valley). Green horizon in part (a) shows the restoration of the present day geometry of the fossil plate interface zone after removal of the vertical offset along the Engadine line (Fig. 2b), whereas the black horizon shows the restored South Penninic domain after unfolding. The tip of the Wägitaler flysch (derived from the Tectonic map of Switzerland 1:500.000, 2<sup>nd</sup> edition, 1980) is used as the minimum distance to the tip of the fossil accretionary prism. Part (b) shows the database for reconstructing the dip of the plate interface zone. Depth determination using different geothermal gradients is based on vitrinite reflectance data, published and own geothermobarometric data, as well as field estimates of deformation temperatures. This resulted in a mean dip angle of 8°. Topographic slope is 5° for the outer wedge, 3° for the inner wedge, and 0° for the portion landward of the shelf edge (based on a mean value given by Moores and Twiss, 1995; Clift and Vannucchi, 2004; Wang and Hu, 2006). The minimum extent of the accretionary prism is again shifted towards the NNW in order to fit the vitrinite reflectance data providing an approximation for overburden north of profile 1. Part (c) presents the final restoration of the plate interface for the time window 89 Ma to 50 Ma and the relocated profiles.





Original Figure is DIN A3 and can be obtained from the author.

show a characteristic downdip change (Figs. 4.7, 4.8a-o). This in particular includes the extent of Alpine deformation of the Austroalpine basement close to the contact to the underlying South Penninic *mélange*, the degree of deformation of the South Penninic *mélange* with increasing metamorphism, the quantity and density of localized deformation zones (LDZ), the occurrence of mylonitic textures within the South Penninic *mélange*, the appearance and deformation of embedded clasts, the proportion of pseudotachylytes, as well as the occurrence and quantity of mineralized vein systems.

#### 4.7.2. Deformation

The degree of penetrative deformation within the study area increases downdip, respectively towards the south (Fig. 4.7). The proportion of individual zones of localized deformation (LDZ) per meter increases from profile 1 to profile 8 in the same way (Figs. 4.7, 4.8a, 4.8b). We used distinct surfaces of up to few millimeters width cutting through the outcrops (almost parallel to foliation) as localized deformation zones (LDZ). Sparsely, we observed offsets along the LDZ reaching up to a few cm (Fig. 4.8c). In carbonate-dominated rocks of the South Penninic *mélange* these zones are mainly expressed by pressure solution seams. However, LDZ might possibly evolve into sites of subsequent preferred pressure solution with progressive deformation. We measured the amount of localized deformation zones in outcrops and images using appropriate scale bars. Within the northern profiles (1-4) the number of localized deformation zones (LDZ) per meter measured in outcrops of the South Penninic *mélange* is low (less than 40 LDZ/m, corresponding to 3% of the outcrop). At profile 5 (450 LDZ/m, corresponding to 45 % of the outcrop) and more obviously at profile 7 (880 LDZ/m, corresponding to 88% of the outcrop), the

amount of LDZ within metasedimentary rocks of the South Penninic *mélange* increases drastically (Fig. 4.7). Due to this high amount of LDZ it is difficult to identify individual LDZ at outcrop scale, and we described the outcrops as completely deformed. There, deformation is distributed over the whole outcrop (e.g. at profile 8 amount of LDZ equals 96% of the outcrop). Thus, the increase in amount of LDZ reflects the transition to a distributed deformation towards the south, where especially the metasedimentary matrix of South Penninic origin is intensely sheared (Fig. 4.8b). In addition, LDZ density seems to be lithology dependent. Ultrabasic clasts are characterized by brittle fracturing in the entire working area. Within these rocks we measured less than 20 LDZ/m with no obvious gradient towards the south. The amount of LDZ depends also on the position of the analyzed outcrops relative to the upper plate base. The closer the outcrop to the boundary zone, the higher the total number of LDZ (Fig. 4.9). Even LDZ of the upper plate reflects this behavior in the first tens of meters. Moreover, where the sedimentary cover of the upper plate is in direct contact to the South Penninic *mélange*, it exhibits about tenfold the number of LDZ compared to the crystalline parts of the Austroalpine nappe stack. However, it is still less than the number of LDZ of the South Penninic *mélange* close to the contact to the upper plate (Fig. 4.9).

The volume of rocks with mylonitic textures within the South Penninic *mélange* and the base of the upper plate (related to the Alpine orogeny) increases towards the south. The first appearance can be recognized at profile 6, where rims of carbonatic clasts embedded in the serpentized matrix are mylonitized. In addition, Permian volcanic rocks building the base of the upper plate in parts of profile 6 are intensely deformed close to the contact to the underlying South

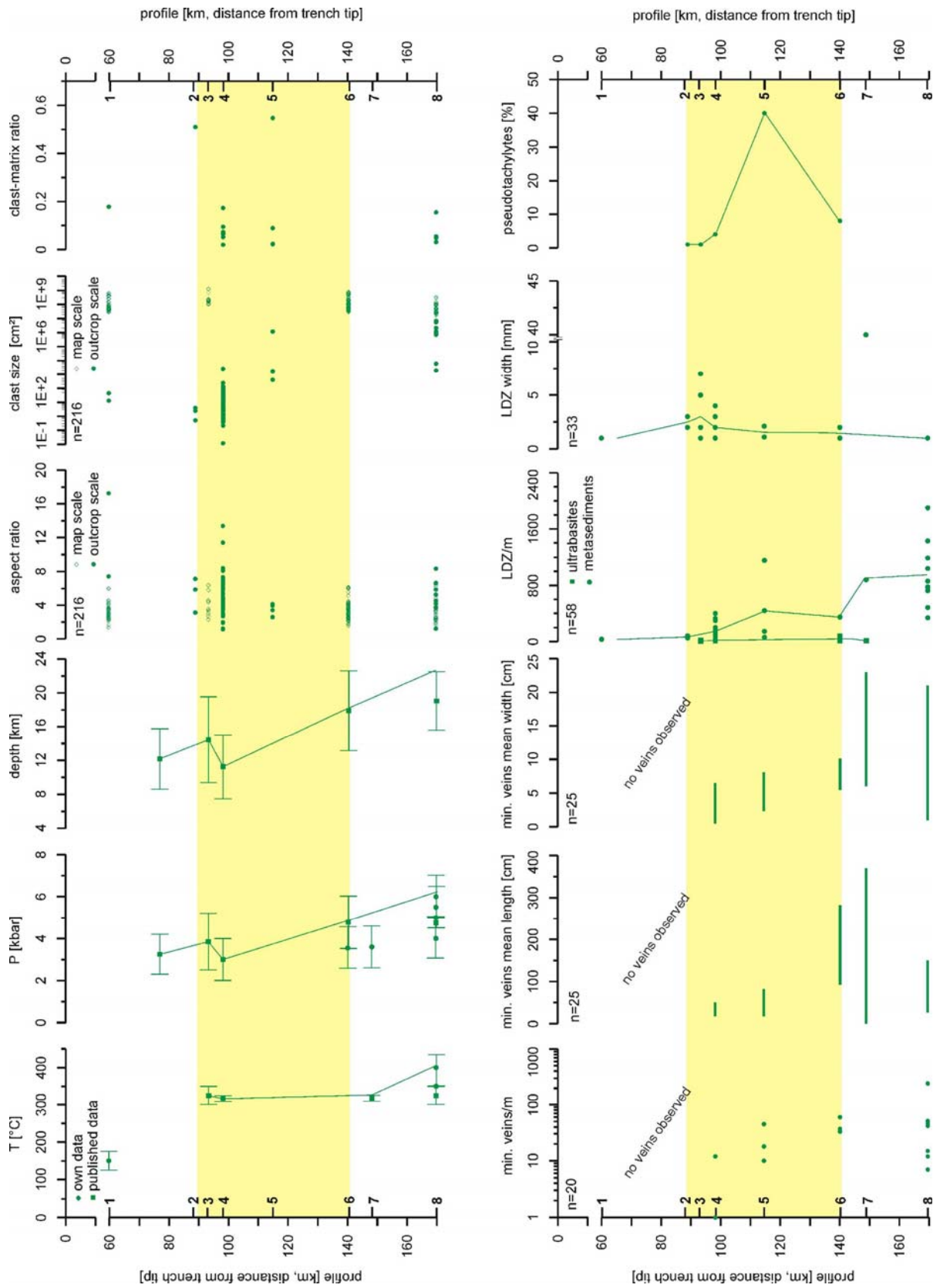


Figure 4.7: Spatial distribution and change of characteristic plate interface zone features. Note, y-axis is corrected using the restored section from Figure 6. Yellow shaded area outlines the extent of the unstable slip region of the fossil seismogenic coupling zone, based on the distribution of pseudotachylytes.



Penninic mélange. At profile 8 also metagabbros as remnants of the South Penninic oceanic crust exhibit mylonitic parts. Limestone layers are deformed to calcmylonites. Crystalplastic deformation of the quartz lattice is dominant towards the south also pointing to activity of slow viscous deformation.

#### 4.7.3. Clasts

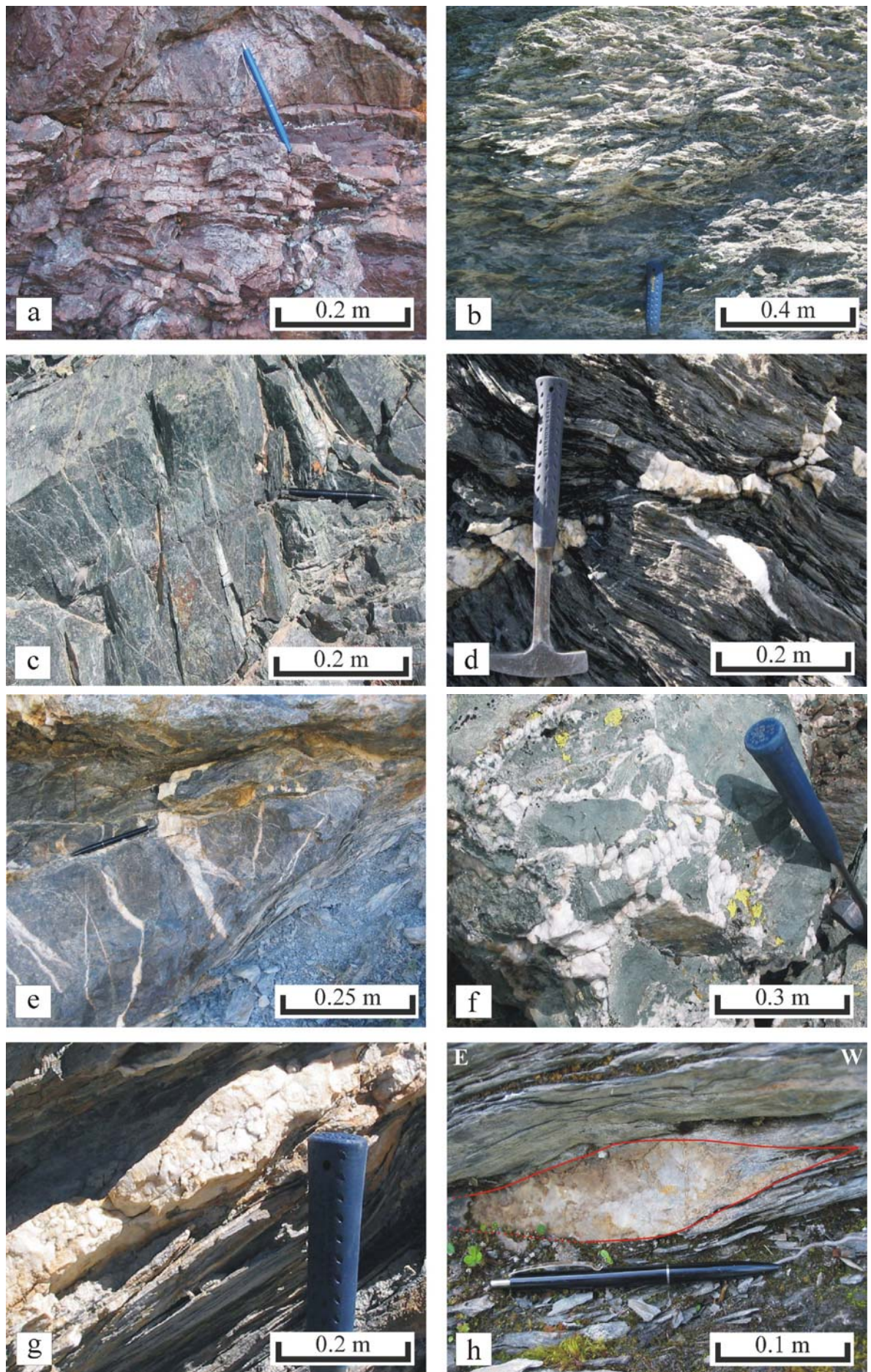
Clast size varies from a few cm up to more than several hundreds of meters (Fig. 4.7). Smaller clasts are nearly completely assimilated into the matrix. Clasts are always oriented with their long axes parallel to the main foliation and their shapes show all transitions between symmetric and asymmetric sigmoidal forms. In general, they mirror the general top-W directed tectonic transport. In order to cover a broad scale of clast sizes we used geological maps presented in Ring et al. (1990) in addition to own outcrop pictures. Note, due to the use of geological maps instead of cross sections, the calculated aspect ratios for map scale clasts represent only minimum values. Aspect ratios for individual clasts are around 5 to 10, which appears to be quite constant for all profiles (Fig. 4.7). There is no obvious contrast between outcrop scale and map scale derived aspect ratios, which indicate that the use of geological maps instead of cross sections is appropriate in our case. The average clast-matrix ratio is about 0.1 and does not change significantly towards the south of the working area (Fig. 4.7). Clast size increases appreciably from the north to the south (Fig. 4.7). The

identification of individual clasts depends strongly on the ratio between clast size and size of the outcrop. In consequence, some clasts are only detectable at map scale. Particularly in the northern part of the working area the identification of individual clasts is problematic. There, outcrops of metasediments or upper plate basement seem to be mega-clasts embedded in a shaly matrix, whereas their boundaries are often not detectable.

Individual layers of sandstone or more pristine carbonates from the sediment pile of the South Penninic ocean are affected by extensional cracking in the north of the working area. With increasing deformation and metamorphism towards the south these layers start to boudinage and progressively separate. Clasts, which are affected by cataclastic deformation in the northern part of the working area, are progressively mylonitized along their rims towards the south. In addition, invading mylonitic shear fractures enforce their disintegration.

#### 4.7.4. Pseudotachylytes

Pseudotachylytes are considered evidence of fossil earthquakes (e.g. Cowan, 1999). These melt veins are formed by frictional heating, preferentially in dry, low porosity rocks, and incorporate angular to subrounded clasts of the wall rock (Sibson, 1975; Spray, 1992). Within the working area pseudotachylytes are present at several localities along the composite N-S section, but are so far found exclusively in the basal section of the crystalline basement of the Austroalpine upper plate (found from the base to a distance of 300m above the base). In addition, we never recognized pseudotachylytes within metasedimentary rocks of the South Penninic mélange, neither in the matrix nor in the clasts. Pseudotachylytes range from mm to several dm in width, and form layers, networks or the matrix of breccia zones (Fig. 4.8i). We determined the



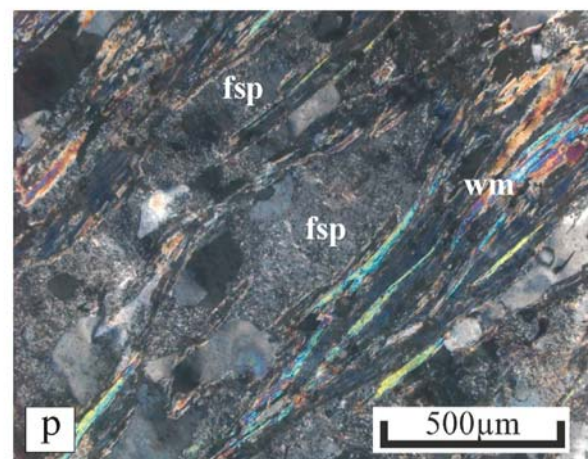
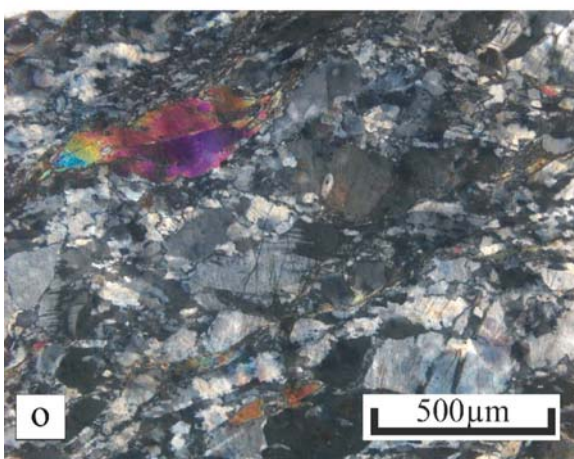
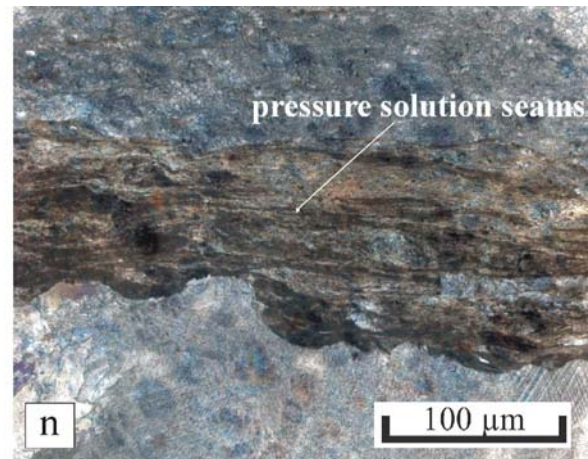
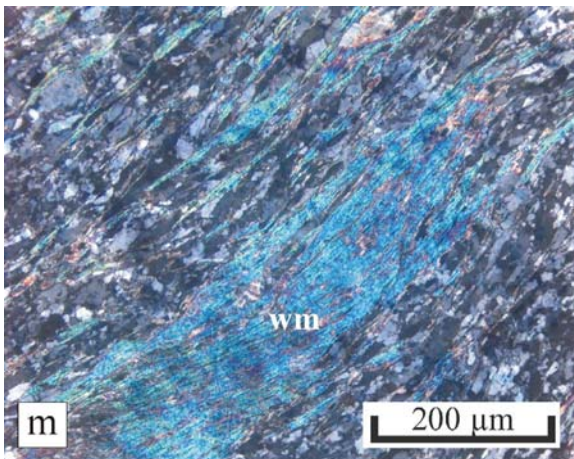
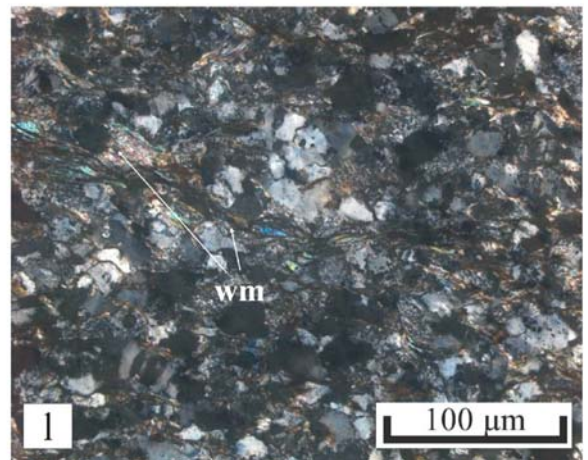
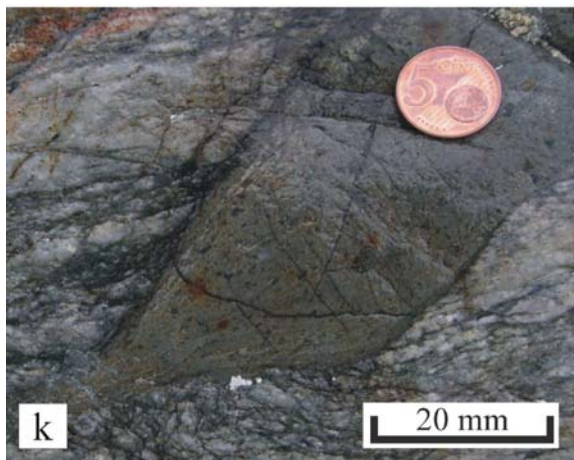
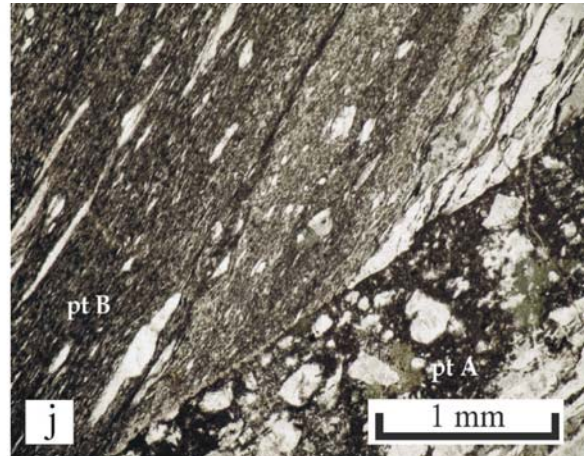
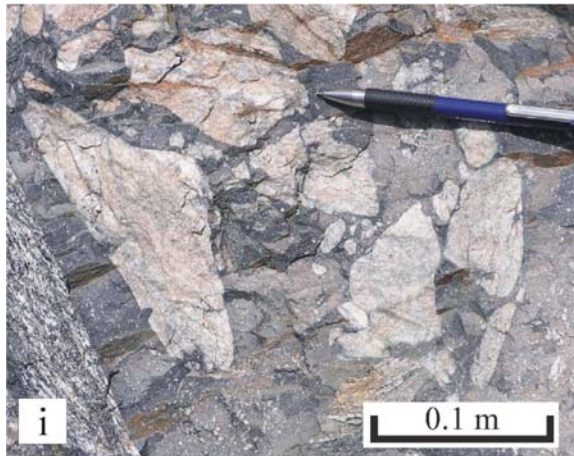


Figure 4.8: Outcrop and thin section images illustrating the change of characteristic features with depth: (a) localized deformation zones (LDZ) in the north of the working area (profile 1), (b) increase in LDZ and distributed deformation over the whole outcrop scale towards the south (profile 6), (c) offset along LDZ in the range of a few cm, (d) mineralized vein subparallel to the foliation and mineralized vein branching off from the main vein, cross-cutting the foliation in a high angle, (e) mineralized vein cutting into competent clast almost perpendicular to its rim, (f) incorporated wall rock fragment within mineralized vein exhibiting a similar texture as pseudotachylytes, (g) mineralized vein running parallel to the foliation and opening into small lentoid fractures, (h) mineralized vein with lentoid shape pointing to top-W hanging wall displacement due to its sigmoidal shape, (i) pseudotachylyte as evidence for unstable slip with incorporated wall rock fragments, (j) mylonitized pseudotachylyte (pt B) cut by a undeformed pseudotachylyte (pt A) pointing to mutual crosscutting relationship between seismic and aseismic deformation, (k) outcrop image of mylonitized pseudotachylyte (alignment of elongated embedded fragments), (l) meta-sandstone with incipient alignment of small white mica and initial formation of foliation (northern part of working area), (m) qtz-mica schist with large white mica aligned within the foliation (southern part of working area), (n) thin section showing pressure solution within deformed limestone, (o) less altered upper plate basement (northern part), and (p) heavily altered upper plate basement (sericitized feldspar with alignment of reaction products) indicating percolating fluids and hydration (southern part).

amount of pseudotachylytes by assessing their relative abundance at outcrop scale (Fig. 4.7). Pseudotachylyte occurrence culminates at profile 5 along the northwestern part of the Engadine window, where partly up to 40% of the outcrops are formed by these melt veins (Fig. 4.7; see also Koch und Masch, 1992; Schmutz, 1995). No pseudotachylytes are found further south than profile 6. At profile 5 we observed an overprint of pseudotachylytes by ductile deformation, maybe promoted by the small grain size of the recrystallized pseudotachylytes favoring viscous grain-size sensitive deformation mechanisms (grain boundary sliding) (Figs. 4.8j, k). In addition, there is a mutual crosscutting relationship between undeformed pseudotachylytes and mylonitized pseudotachylytes (Fig. 4.8j). The wall rock hosting the pseudotachylytes (Austroalpine basement) does not exhibit an Alpine mylonitic overprint. Mylonitic deformation is rather assigned to the higher grade amphibolite facies metamorphism during Variscian orogeny (due to the mineral composition of the mylonitic rocks) (Schmutz, 1995), a metamorphic grade, which was not reached during Alpine orogeny. Chapter 5 deals with pseudotachylytes in more detail.

#### 4.7.5. Mineralized veins

From profile 4 towards the south, the metasedimentary matrix, the metabasic rocks of the South Penninic *mélange*, and dolomite clasts exhibit an increasing amount of mineralized veins, whereas they are rare within the upper plate base throughout the working area (Fig. 4.7). However, an intense alteration of mica and feldspar crystals to chlorite and sericite is widespread in the upper plate basement indicating hydration from percolating fluids. The timing of alteration, however, is not constrained (Fig. 4.8k). The mineralized veins within rocks of the South Penninic *mélange* are generally oriented parallel to sub-parallel to the foliation and fill dilational jogs (mirror top-W hanging wall displacement, Fig. 4.8h), or they cut into more competent clasts embedded in the shaly or serpentized matrix at a high angle to their rims (Fig. 4.8e). Vein filling has a blocky texture of large minerals mostly formed by quartz and calcite, indicative for growth from a free fluid phase into a wide open cavity (Fig. 4.8f, Yardley, 1984; Nüchter and Stöckhert, 2007). In addition, the incorporation of wall rock fragments within the mineralized veins with no or minor contact to the wall rock supports rapid crystallization. Most obviously at

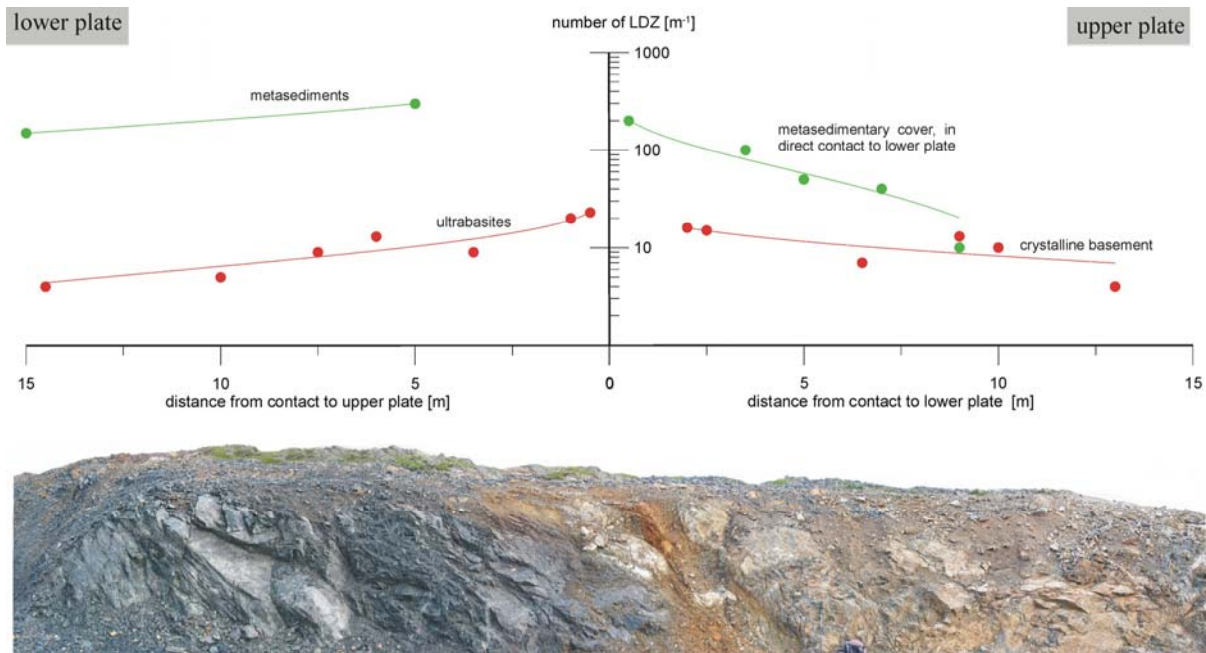


Figure 4.9: Distribution of localized deformation zones (LDZ) along a profile crossing the boundary between the South Penninic domain (lower plate, left side of the figure) and the Austroalpine domain (upper plate, right side of the figure). There is a drastic increase of LDZ towards the base of the upper plate. Therefore, increase in LDZ is not only depth- and lithology-dependent, but also dependent on the distance of the outcrops from the upper plate base as the most prominent shear zone.

profile 5, foliation-parallel mineralized veins within stronger deformed parts of the subduction mélangé are composed of fine-grained dynamically recrystallized calcite. This points to their synkinematic formation with respect to the activity of surrounding shear zones (parallel to the foliation) within the subduction mélangé. Furthermore, veins filled with coarser-grained blocky calcite crystals form either chaotic fracture network or branch off from shear planes with C'-type geometry and cross-cut the foliation at a higher angle (Fig. 4.8d).

Later folds uniformly affect both the foliation and the mineralized veins, which additionally points most likely to vein formation synkinematically to the foliation development. A subsequent set of mineralized veins, unaffected by folding, cuts almost perpendicular to the foliation and the previous veins, and is expressed by a fibrous growth of mostly calcite minerals. These later veins should have

been formed subsequently to the overall deformation along the fossil plate interface.

In order to detect changes in the amount of foliation parallel veins we measured their quantity either directly within outcrops counting them on a tape-measure, or using outcrop images and appropriate scale bars (Fig. 4.7). There are no mineralized veins observable within profiles 1, 2 and 3. At profile 4 and further towards the south the number of foliation parallel veins, as well as their mean length and width, increase (~6 mineralized veins/m at profile 4 and ~55 mineralized veins/m at profile 8; Fig. 4.7) with maximum spread of values south of profile 6. Hence, the trend of increased veining with blocky filling mimics the trend of LDZ density including increasing local variability. In addition, veining in the South Penninic mélangé approximately starts with the occurrence of pseudotachylytes in the basal upper plate, but appears anticorrelated towards and

below the deepest occurrence of pseudotachylytes.

## 4.8. Discussion

### 4.8.1. Post-accretion changes

We rearranged the structural data indicating a pervasive general top-W directed tectonic transport by rotating them into the restored composite section along downdip of the plate interface (rotation axis trends E-W and plunges  $0^\circ$ , rotation angle  $8^\circ$  corresponding to the estimated mean decollement angle, Fig. 4.10). Thereby, the structural data retained their general top-W direction of tectonic transport. At most, measured features such as foliation planes and stretching lineation steepened at the restored dip angle of the plate interface (Fig. 4.10). Furthermore, restoration does not provide hints for a major overprint of the pattern of subduction related metamorphism by younger events exceeding the estimated limits of error (at least 2 kbar vertical, and 5 km horizontal concerning the position of the samples relative to the profiles). All later offsets visible within the section from Schmid et al. (1996) are below 1 km, except for the Engadine line. This is also in agreement with our field observations missing a penetrative overprint of the general top-W directed tectonic transport, which was also reported by Ring (1989) and Dürr (1992).

Nevertheless, the present day fossil subduction channel has been influenced by post-subduction and post-accretion processes during ongoing convergence between both plates. These processes may have involved either both the South Penninic domain and the Austroalpine nappe stack, or only reactivated the direct contact between the lower and the upper plate. Post-subduction shortening of the interface zone would have shifted the

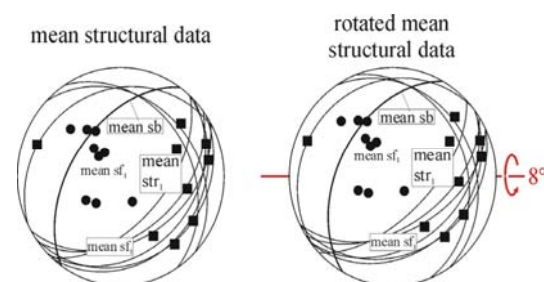


Figure 4.10: Structural data of brittle-ductile to ductile deformation associated with top-NW to top-SW direction of tectonic transport (generally top-W) rotated into the restored composite section perpendicular to the former strike of the plate interface. All plots are Schmidt net lower hemisphere, equal-area diagrams. Note, the structural data retained their general top-W direction of tectonic transport, only e.g. foliation planes and stretching lineation steepened at the restored dip angle of the plate interface.

investigated profiles closer together steepening the dip of the subduction megathrust. Consequently, the estimated megathrust dip would represent a maximum value. In contrast, extension will increase the distance between the analyzed profiles leading to a lower dip angle of the plate interface, and to a minimum megathrust dip angle. In addition, post-subduction motion only along the contact between the South Penninic mélangé and the Austroalpine upper plate would alter the spatial relationship between characteristic features observed along both sides of the suture. NNW-SSE shortening, extension, and displacement on the plate interface have been observed (see e.g. large-scale folding of section). But magnitudes of subsequent deformation are small with respect to the total length and minimum displacement along the plate interface (i.e.  $>170\text{km}$ ), and may even largely cancel out. Moreover, the here calculated dip angle of the plate interface of  $\sim 8^\circ$  is in good agreement with published mean megathrust angles (Lallemand et al., 1994; Moores and Twiss, 1995; Clift and Vannucchi, 2004). In consequence, we consider later modifications irrelevant for the here investigated subduction-related deformation.

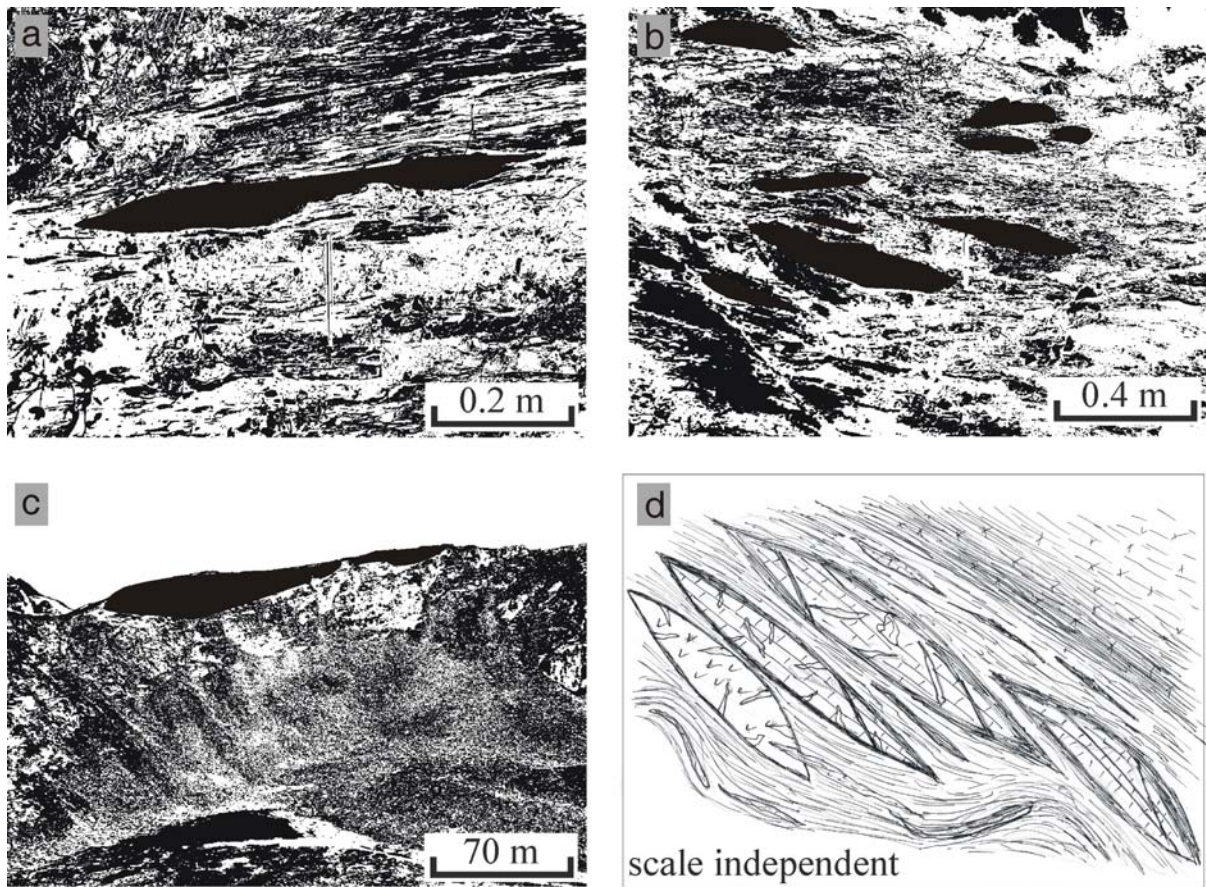


Figure 4.11: Clasts of different size and material are incorporated within the shaly or serpentized matrix. They are elongated with their long axis pointing towards the inferred direction of pervasive tectonic transport, independent of their individual size. This scale independence is shown using outcrop photographs. Clasts are highlighted with the image processing software Scion Image. a) Carbonate clast embedded in shaly matrix at profile 4, b) Carbonate clasts within calcareous and shaly matrix, c) upper plate dolomite clast embedded within subduction mélangé at profile 8, d) shows a representative scale independent synthetic section of clasts and matrix.

#### 4.8.2. Long-term kinematics - tectonic erosion vs. accretion

Clasts within the matrix of the subduction mélangé provide hints for processes such as tectonic erosion and accretion along the plate interface zone. The strong contribution of upper plate fragments (basement and cover) is a diagnostic criterion for the role of tectonic erosion from the base of the upper plate (Oncken, 1998). Tectonic erosion as a key factor controlling the material input into the fossil subduction channel also explains the lack of upper plate crystalline basement immediately above the plate interface in

some parts of the working area, where upper plate sediments directly rest on the mélangé (see also Wagreich, 1995, on reinterpretation of Gosau basins as indicating Late Cretaceous subduction erosion). Basal subduction erosion as prevailing mass transfer mode invariably stopped upon underplating of the mélangé, and abandonment of the subduction of the South Penninic ocean (see also Chapter 6).

The process of layer separation, single clast formation, and later assimilation promoted by invading mylonitic shear fractures (see Chapter 4.7.3) would lead to an increase of the aspect ratio as long as the clasts are detectable as independent

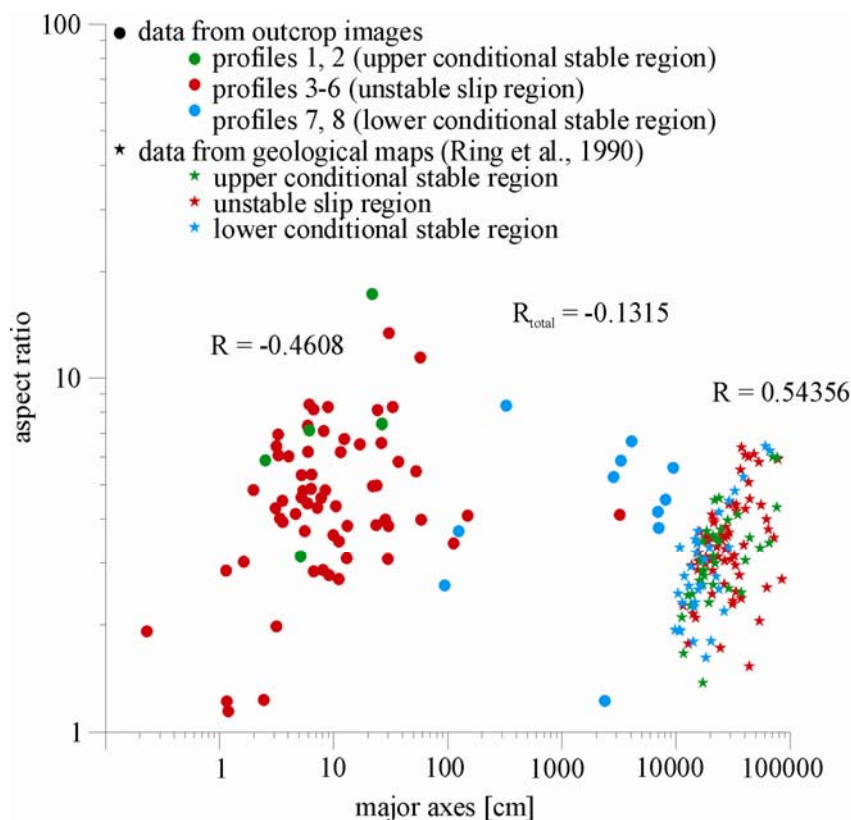


Figure 4.12: Aspect ratio of embedded clasts plotted against major axes. Green dots represent data obtained from outcrop images corresponding to profiles located in the upper conditional stable region, red dots correspond to profiles located within the unstable slip region, whereas blue dots are related to profiles located in the lower conditional stable region. Green stars correspond to data gained from geological maps (Ring et al., 1990) for profiles situated within the upper conditional stable region, red for profiles within the unstable slip region, and blue corresponds to profiles in the lower conditional stable region. There is no obvious trend, expressed by the correlation coefficient  $R$ . Therefore, aspect ratio of clasts is independent of clast size; no hint of the clast's relative position along the fossil plate interface zone is given by a change of the aspect ratio.

objects, and to a decreasing average clast size. An incipient assimilation was observed for both clast types, either slivers of the upper and lower plate or boudinaged clasts of sedimentary layers. But the calculated aspect ratio of individual clasts exhibit no relevant change with depth as would be expected from progressive disintegration (see scale independence of clasts in Fig. 4.11). Additionally, there is no correlation between aspect ratio and clast size (expressed by clasts major axes, Fig. 4.12) suggesting the independence of the aspect ratio compared to the position of the profile along the fossil plate interface, even when taking the limitations by the use of geological maps into account. At most, the average clast size increases towards the

south of the working area (Chapter 4.7.3., Figs. 4.7, 4.12). In all, these observations suggest continuous addition of new clasts from fragmenting the base of the upper plate towards depth indicating tectonic erosion along the entire base of the exposed upper plate and preferential disintegration of smaller fragments until the onset of underplating (Eocene).

A final aspect resulting from long-term material flux merits mentioning: Because of more or less continuous flux of the material in the subduction channel, all features will be displaced downdip once formed, or even updip due to return flow. This will result in (1) offset of mélangé features with regard to the overlying

features at the base of the upper plate (except for first occurrence of features); to (2) an apparent downdip increase in key features when continuously formed during downdip flow; to (3) apparently gradational boundaries that may have been more distinct during formation. None of these aspects will be of significance in the upper plate. The apparent linear increase of e.g. the number of LDZ within the subduction mélange and mineralized veins potentially supports the interpretation of continuing formation paralleling the post-formation displacement of key features towards depth during long-term material flux.

#### *4.8.3. Short-term kinematics - unstable slip vs. stable sliding*

To this date, pseudotachylytes are considered the only unambiguous evidence for faulting at seismic velocities (e.g. Cowan, 1999). Therefore, we interpret their occurrence along the exhumed plate interface as delineating the area of unstable slip (yellow shaded area within Fig. 4.7). From the northernmost occurrence of pseudotachylytes we identify the fossil updip limit of unstable sliding close to profile 2 at a distance of ~90 km from the trench corresponding to a depth of ~15 km, and a temperature of ~200°C (temperature estimate based on deformational behavior of different minerals, see Chapter 4.5.2, Fig. 4.13). Correspondingly, the southernmost occurrence of pseudotachylytes defines the fossil downdip limit of unstable slip, and is located close to profile 6 at a distance of 140 km from the trench equivalent to a depth of ~22 km, and a temperature of ~300°C (temperature estimate based on deformational behavior of different minerals, see Chapter 4.5.2, Fig. 4.13). The conditionally stable segments above and below the unstable segment may continue for some distance up-, but also downdip. Several observations point to the

coincidence of the downdip limit of unstable slip with the start of a transitional zone at the downdip limit of the seismogenic coupling zone (transition from seismic to aseismic and conditionally unstable slip): the observed mylonitic overprint of pseudotachylytes, the mutual crosscutting of overprinted and non-overprinted pseudotachylytes at profile 5 (see Chapter 4.7.4.), the drastic increase in LDZ (see Chapter 4.7.2.), and the onset of mylonitic rocks in the subduction mélange and, slightly deeper, at the base of the upper plate (Fig. 4.13).

Below the downdip end of unstable slip we observe a continuing increase of LDZ in the mélange, progressively observed as distributed over the scale of the whole outcrop (Chapter 4.7.2., Figs. 4.7, 4.8b), jointly occurring with mylonites. This continuous increase requires formation of localized deformation zones that may be seismic also below the zone of unstable slip, when they compete with ductile shearing. Hence, we suggest seismic behavior to be possible in the subduction mélange to temperatures of at least 300°C to 350°C and possible higher. However, formation of LDZ and therefore seismic behavior is strongly lithology dependent (see Chapter 4.7.2, Fig. 4.11). The transition between seismic and aseismic deformation in our studied example is well comparable to the proposed transitional zone downdip of the seismogenic part of active convergent plate interfaces (e.g. Hyndman and Wang, 1995). There, seismic slip in the transitional zone may occur during major coseismic events rupturing the entire unstable slip zone, subsequently overprinted by viscous deformation during postseismic relaxation and interseismic creep. However, we note that recent observations of silent slip events (slip velocity at ~0.1 m/s, Schwartz and Rokosky, 2007) have been reported for the transitional zone. Our observations may well also relate to this observation.

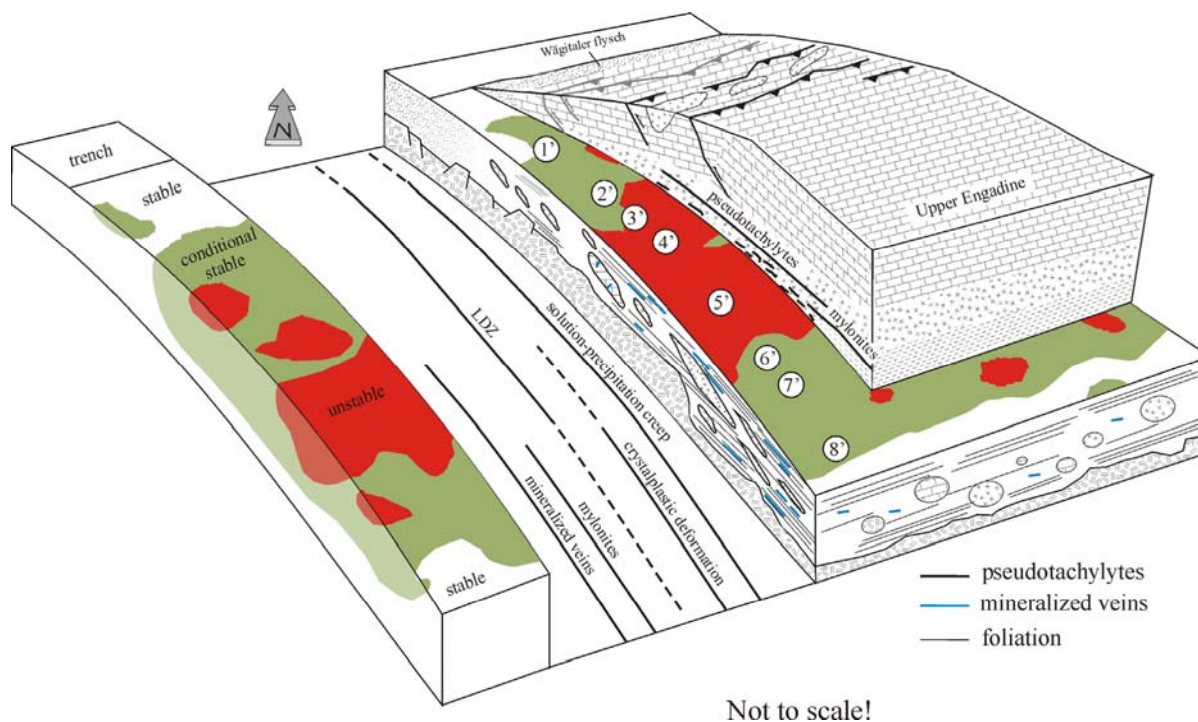


Figure 4.13: Final interpretative section showing the profile positions, as well as the association and interference of the discussed key features. Solution-precipitation creep is dominant in all of the study area, whereas crystalplastic deformation appears towards the south. The number of LDZ increase downdip the plate interface, and in the southern part of the working area the South Penninic mélangé is deformed over the scale of the whole outcrop, closely associated with mylonites. Pseudotachylytes occur within a certain depth range along the fossil plate interface immediately above the base of the upper plate basement delineating the former unstable slip region within the seismogenic coupling zone. Above and below the unstable slip region areas of conditional stability occur, characterized by the coexistence of slow deformation (e.g. solution-precipitation creep in the northern part of the working area, crystalplastic deformation in the southern part) and maybe seismic deformation (e.g. LDZ, mineralized veins). The regions of stable, conditional stable and unstable slip will vary in space and time in accordance to spatiotemporal variance in e.g. sediment input, dewatering and dehydration. Thus, the mechanical conditions within the subduction channel are not characterized by steady state behaviour. Mineralized veins are spatially associated with pseudotachylytes, but exclusively found within the subduction mélangé. This fact points to different rheological behaviour of the subduction mélangé and the crystalline basement of the upper plate. The former prevent the built-up of high effective normal stress and associated shear stress by ongoing hydraulic fracturing and the latter enables the accumulation of higher effective normal stress and associated shear stress. From the spatial coincidence of both pseudotachylytes and mineralized veins and their identical texture we suggest that formation of this type of veins in the subduction channel potentially indicates unstable slip. Model of frictional conditions modified and extended downdip following Bilek and Lay (2002).

The updip extent of the fossil seismogenic coupling zone is probably much wider than the zone of unstable slip outlined by the occurrence of pseudotachylytes. This assumption is supported by the fact that the here estimated updip limit of unstable slip (~15 km depth, 200°C) is below the widely accepted values for the updip limit of the seismogenic coupling zone of active convergent plate margins (~5 km depth, 100°C-150°C, e.g. Oleskevich et al.,

1999). Additionally, we observed localized deformation zones northward (i.e. trenchward) of the estimated upper limit of the unstable slip area. They may also point to slip localization during potentially coseismic events. Otherwise, pressure solution seams, which are widespread in the northern part of the working area, are evidence for aseismic creep (e.g. Kitamura et al., 2005), possibly prevailing in the postseismic relaxation period.

Patches of stable, unstable and conditional stable behavior might change their location not only in space, but also in time. This is caused by spatiotemporally dependent processes, such as compaction, dewatering and dehydration, which influence the frictional properties within the subduction channel. These processes are strongly dependent on other spatiotemporal variable factors, for example the composition and the amount of sediment input, as well as the temperature regime. This variance in space and time might additionally smear out possible distinct boundaries concerning the onset of plate interface key features. This should be of larger influence for features along the upper plate base (e.g. pseudotachylytes resulting from frictional instability within the subduction channel), as the upper plate base is relatively fixed with respect to the material moving within the subduction channel. Otherwise, the effect may be negligible for the subduction channel matrix itself due to the superimposition of continuing downward transport of key features by continuous material flux, which also leads to apparently gradational boundaries (see Chapter 4.8.2). In consequence, the plate interface zone cannot exhibit a steady state behavior.

#### *4.8.4. Fluid flow and constraints for long- and short-term deformation*

Evidence for fluids circulating along the plate interface are widespread in the working area. This is indicated by the ubiquitous presence of foliation-parallel mineralized vein systems in the *mélange* matrix (Fig. 4.8d), and by veins cutting into competent clasts both downdip of profile 4 (Fig. 4.8e, Chapter 4.7.5.). The presence of fluids is also necessary for the observed solution-precipitation creep as dominant deformation mechanism in all of the study area (Fig. 4.8g), including the zone updip of profile 4 (Fig. 4.13). From the absence of mineralized veins updip of

profile 4 we conclude that fluid percolation must have occurred unimpeded through a permeable fracture network, along foliation planes and grain boundaries in the conditionally stable domain (Fig. 4.13). Starting only in the unstable slip domain, formation of mineralized veins clearly requires fluid production rate to exceed percolation rate through an open system building near-lithostatic fluid pressure during parts of the seismic cycle. The hampered fluid flow might be in line with an increase in upper plate alteration and growth of sheet silicates along foliation planes within the subduction *mélange*.

Increasing fluid pressure lowers the effective normal stress, and thus triggers the formation of cracks (e.g. Hubbert and Willis, 1957; Hubbert and Rubey, 1959; Secor, 1965; Sibson, 1981; Atkinson, 1987). According to Husen and Kissling (2001) an increase in fluid pressure is promoted by the concentration of high stress along the plate interface, which leads to sealing, and thus to trapping of fluids. Major earthquakes are thought to be able to break this seal, thus allowing fluids to migrate upwards along the gradient in fluid pressure (hydrostatic fluid pressure above the seal, lithostatic fluid pressure below the seal). This coincides well with our observations that mineralized veins were restricted to rocks within the deeper portions of the subduction channel (South Penninic *mélange*), whereas clear evidence for mineralized veins are missing within the upper plate. However, an intense alteration of mica and feldspar minerals is widespread at the base of the upper plate (Fig. 4.8o). Although, the timing of alteration is poorly constrained, the reaction products may be aligned in a younger foliation of presumable Alpine age in the more southern parts. Alteration processes lead to a consummation of dehydration fluids. Additionally, the observed foliation development makes the base of the upper plate an efficient seal. Within the subduction *mélange* the growth

of sheet silicates (white mica, chlorite, Figs. 4.8l, m) also consumes fluids. In addition, mylonitic overprint of pseudotachylytes immediately above the base of the crystalline hanging wall may also be supported by some fluid circulation enhancing devitrification, formation of hydrate phases, and grain boundary sliding (Fig. 4.8j).

The blocky texture of minerals, which fill the foliation-parallel veins (Fig. 4.8g) starting from the updip end of the unstable slip domain, indicates that fracture opening was faster than mineral growth. Furthermore, this blocky texture is suggested to point to ongoing nucleation during supersaturation of vein-forming minerals (Oliver and Bons, 2001). According to these authors, this might be expected for faults, which exhibit a large, near-instantaneous fluid pressure drop upon fracturing. Nüchter and Stöckhert (2007) concluded that fracturing and cavity formation could reflect a cycle of instantaneous loading followed by stress relaxation within a very short time span. This could point to fluid-induced seismicity or to seismically triggered hydrofracs. However, the relationship of these mineralized veins to deformation at seismic velocities (in the range of 1m/s and more; Cowan, 1999) has yet to be evaluated. Nevertheless, the internal structure of the mineralized veins resembles the structure of pseudotachylyte networks, which are clear evidence for unstable slip (Figs. 4.8f, i). Embedded wall rock fragments within the mineralized veins and within the pseudotachylytes - either without or with minor contact to the wall rock (Figs. 4.8f, i) - point to fast fracturing and subsequent rapid solidification processes. Therefore, from the spatial coincidence of both features (Fig. 4.13) and their identical texture we suggest that formation of this type of veins in the subduction channel potentially indicates unstable slip.

In spite of their mutual association to the seismic process, we conclude that the exclusive restriction of pseudotachylytes and mineralized vein systems to one component of the plate boundary system - i.e. base of upper plate vs. *mélange* - is most likely due to a different rheological behavior of both, the sedimentary matrix of the subduction channel, and the crystalline basement of the upper plate. Fluids within the *mélange* (sealed from above) prevent the built-up of high effective normal stress and associated shear stress by ongoing hydraulic fracturing, hence cause a lower potential for shear heating. In contrast, crystalline upper plate rocks (drained from above) support higher effective normal stress and associated shear stress, a prerequisite for the formation of shear fractures and frictional heating, and thus for pseudotachylytes. The mechanical and kinematical key role of the base of the upper plate as the most prominent shear zone is not only underscored by the highest density of pseudotachylytes immediately above the contact, but also by the highest number of LDZ immediately above and below this boundary (Fig. 4.10).

Extensional veins sub-parallel to cleavage formed by compression and/ or shear require variations or a switch of stress directions as well as of the state of fluid pressure. This explains the development of mineralized veins sub-parallel to the maximum compression direction associated with foliation. Transient changes of the state of stress, as expected for repeated seismic loading cycles, may particularly facilitate the development of foliation-parallel veins. In principle, opening of fractures occurs when the minimum principle stress equals the tensile strength of the rock. As proposed in the accretionary model of Meneghini et al. (2007), the stress parallel to subducted sedimentary layers should be larger than the stress normal to the bedding, which is plausible at shallow subduction dip angles, and would promote layer-parallel veining.

In addition, seismically controlled stress cycles at elevated and equally transient fluid pressure lead to the alternating development of foliation-parallel and foliation-normal veins (e.g. Meneghini et al., 2007). In the study presented here, veins parallel to the sedimentary layering are widespread (Fig. 4.8d), whereas veins approximately normal to the sedimentary layering are mainly observed in competent clasts (Fig. 4.8e). However, best developed at profile 5, there are veins filled with blocky calcite crystals, which cross-cut the foliation at a higher angle (branching off from shear planes with a C'-type geometry, Fig. 4.8d). These veins might represent transient upward directed fluid injections resulting from a cyclic build-up of fluid pressure during burial of sediments, dewatering and dehydration (Meneghini et al. 2007). The common observation of foliation-parallel mineralized veins within the subduction mélange of the study area provides hints for the occurrence of pathways for layer-parallel fluid release and transport as required in the model of Meneghini et al. (2007). The heterogeneous internal structure of the subduction mélange governs the transport of released fluids both along and across the foliation, foliation parallel shear planes, and thus, the plate interface. In conclusion, we assume shear deformation and persistent changes of the stress field by cyclic fluid pressure to operate contemporaneously or alternately leading to vein formation synkinematically to the development of foliation.

Last but not least, we note that the abundance of veins increases downdip to the base of the unstable slip zone. Hence, veining therefore probably proceeded along this entire segment. Its geometric style changes deeper down with longer and wider veins, still indicating ongoing hydrofracturing in the lower conditionally stable zone as also observed for the LDZ.

#### 4.9. Conclusions

We analyzed a continuous exposure exhibiting the complete seismogenic part of a subduction channel and its upper plate hanging wall within the Central Alps of Europe. For this purpose we restored the fossil plate interface zone to its subduction geometry resulting in a 170 km long section with a ca. 8° SSE-dipping plate interface for the Late Cretaceous to Eocene period prior to the collision and underplating of the continental Briançonnais domain. During subduction of the South Penninic ocean, material from different sources (continental upper plate, oceanic lower plate) was progressively involved into the subduction factory and transported downwards, forming either the shaly and serpentinitic matrix of the subduction mélange, or competent clasts. Tectonic erosion controlled mass transfer within the subduction channel during the Late Cretaceous to Eocene, while subsequent basal accretion lead to the abandonment of this major shear zone. The internal structure of the studied fossil subduction channel resembles the proposed internal structure of active systems inferred from e.g. seismic and seismological data: less deformed units are bounded by a network of active shear zones or sheared matrix. Therefore, preservation of sedimentary and/ or magmatic textures in blocks of all sizes is supported, unless deformation affects the whole subduction mélange.

Along the SSE-dipping plate interface overprint of the upper plate base by Alpine deformation increases towards depth (respectively towards the south of the working area). The matrix of the subduction channel exhibits an equally increasing deformation and metamorphic grade, and the number of mylonitic shear zones and mylonitic rocks progressively increase as well (including the onset of crystalplastic deformation). The density of LDZ also increases downdip ultimately

involving the entire subduction channel matrix.

Pseudotachylytes along a restricted segment of the upper plate base – delineated by ca. 200°C updip and ca. 300°C downdip – define the limits of the unstable slip region within the fossil seismogenic coupling zone. Foliation-parallel mineralized veins with partly blocky mineralization that occur over the same depth range, but continue to below the unstable slip domain, are suggested to reflect seismic failure in the subduction mélangé. The existence of mineralized veins requires fluid production rate exceeding fluid percolation rate, and the thereby caused built up of lithostatic fluid pressures. Growth and alignment of sheet silicates (white mica, chlorite) along foliation planes clearly hampers the percolation of fluids through a co- to postseismically open system that is progressively compacted and cemented during the post- to interseismic stage. In addition, starting from the unstable region downdip, the plate interface zone is characterized by an impermeable upper plate due to fluid assisted alteration processes and fabric development. Therefore, the region of unstable slip within the seismogenic coupling zone has an at least intermittently lithostatic fluid regime effectively sealed off from the higher parts of the subduction channel as well as from the overlying wedge by the hydrated and impermeable upper plate base. Fluid flow supports both long-term interseismic and short-term coseismic deformation by enhancing solution-precipitation creep, mylonitization of pseudotachylytes (by enhancing devitrification, hydrate phase formation, grain boundary sliding) and fracturing, respectively, in the unstable slip zone as well as in the deeper transitional zone. The upper conditionally stable zone shows abundant evidence for brittle localized fracture, but no indication for hydraulic fracturing. The corresponding fluid regime

is sub-lithostatic and probably dewateres the plate interface through an interconnected fracture network, along foliation planes or grain boundaries. The circulation of fluids is indicated by solution-precipitation creep as the dominant deformation mechanism. The lower conditionally stable region is again characterized by hampered fluid flow indicated by the increasing number of mineralized veins even below the unstable slip zone. This may possibly indicate a domain of slow earthquakes and non-volcanic tremors as recently discovered for this depth range along many active convergent margins.